



HAL
open science

Intrabody induced cell death by targeting the *T. brucei* cytoskeletal protein TbBILBO1

Christine E Broster Reix, Miharisoa Rijatiana Ramanantsalama, Carmelo Di Primo, Laëtitia Minder, Melanie Bonhivers, Denis Dacheux, Derrick R Robinson

► To cite this version:

Christine E Broster Reix, Miharisoa Rijatiana Ramanantsalama, Carmelo Di Primo, Laëtitia Minder, Melanie Bonhivers, et al.. Intrabody induced cell death by targeting the *T. brucei* cytoskeletal protein TbBILBO1. *Microbiology Spectrum*, In press. hal-03367221v1

HAL Id: hal-03367221

<https://hal.science/hal-03367221v1>

Submitted on 6 Oct 2021 (v1), last revised 27 Jan 2022 (v2)

HAL is a multi-disciplinary open access archive for the deposit and dissemination of scientific research documents, whether they are published or not. The documents may come from teaching and research institutions in France or abroad, or from public or private research centers.

L'archive ouverte pluridisciplinaire **HAL**, est destinée au dépôt et à la diffusion de documents scientifiques de niveau recherche, publiés ou non, émanant des établissements d'enseignement et de recherche français ou étrangers, des laboratoires publics ou privés.

Authors and affiliations

Title: Intrabody induced cell death by targeting the *T. brucei* cytoskeletal protein *TbBILBO1*

Short title: Intrabody-induced trypanosome cytoskeleton disruption

Christine E. Broster Reix^{\$1}, Miharisoa Rijatiana Ramanantsalama^{\$1}, Carmelo Di Primo², Laëtitia Minder^{2,3}, Mélanie Bonhivers¹, Denis Dacheux^{1,4}, Derrick R. Robinson^{1*}.

¹University of Bordeaux, CNRS, Microbiologie Fondamentale et Pathogénicité, UMR 5234, F-33000 146 rue Léo Saignat, Batiment 3A - 1^{er} étage, 33076 Bordeaux, France.

²University of Bordeaux, INSERM U1212-CNRS UMR 5320, ARNA laboratory, European Institute of Chemistry and Biology, 2 rue Robert Escarpit, 33607 Pessac cedex, France.

³University of Bordeaux, CNRS UMS3033-INSERM US001, European Institute of Chemistry and Biology, 2 rue Robert Escarpit, 33607 Pessac cedex, France.

⁴Bordeaux INP, Microbiologie Fondamentale et Pathogénicité, UMR 5234, F-33000 Bordeaux, France.

\$ Shared first authors

*Author for correspondence

24 **Abstract**

25

26 *Trypanosoma brucei* belongs to a genus of protists that cause life-threatening and economically
27 important diseases of human and animal populations in Sub-Saharan Africa. *T. brucei* cells are cov-
28 ered in surface glycoproteins some of which are used to escape the host immune system. Exo-
29 /endocytotic trafficking of these and other molecules occurs *via* a single copy organelle called the
30 flagellar pocket (FP). The FP is maintained and enclosed around the flagellum by the flagellar
31 pocket collar (FPC). To date, the most important cytoskeletal component of the FPC is an essential,
32 calcium-binding, polymer-forming protein called *TbBILBO1*. In searching for novel immune-tools
33 to study this protein, we raised nanobodies (Nb), against *TbBILBO1*. Nanobodies were selected
34 according to their binding properties to *TbBILBO1*, were tested as immunofluorescence tools and
35 expressed as intrabodies (INb). One of them, Nb48, proved to be the most robust nanobody and
36 intrabody. We further demonstrate that inducible, cytoplasmic expression of INb48 was lethal to
37 these parasites, producing abnormal phenotypes resembling those of *TbBILBO1* RNAi knockdown.
38 Our results validate the feasibility of generating functional single-domain antibody derived intra-
39 bodies to target trypanosome cytoskeleton proteins.

40

41 **Introduction**

42

43 Trypanosomes are flagellated protists comprised of pathogenic species capable of infecting a wide
44 range of vertebrate hosts including humans, domestic and wild animals. Commonly transmitted by
45 insect vectors, trypanosomes cause lethal and economically important human and animal diseases
46 worldwide (1, 2). A limited number of diagnostic tests and treatments are available for human and
47 animal African trypanosomiasis and there are no vaccines. Fortunately, the first oral trypanocidal
48 drug, Fexinidazole, was recently approved for use in humans in Africa (3, 4) which simplifies the
49 treatment regime for certain cases. However, millions of wild animals and domesticated livestock
50 are still at risk of infection with the economic burden of the disease to the African economy is esti-
51 mated to be 4.7 billion USD per year due to the death of around 3 million head of cattle (5)
52 (<http://www.fao.org/paat/the-programme/the-disease/en/>). Understanding the basic biology of any
53 virulent organism is important to fully understand its pathogenicity. Furthermore, new targets, tools,
54 and models are needed.

55

56 Trypanosomes possess a highly organized cytoskeleton comprised primarily of microtubules, but
57 also many cytoskeleton-associated proteins (5–13). This ensemble of proteins coordinates changes
58 in cell morphology during the cell cycle, as well as permitting cell motility and reorganization dur-
59 ing differentiation between life-cycle stages. Most pathogenic trypanosomes possess a single copy
60 organelle called the flagellar pocket (FP), an infolding of the pellicular membrane at the site where
61 the flagellum exits the cell body, which is physically connected to the cytoskeleton (13–18). In
62 many species the FP is the sole site of exo- and endocytosis. In *T. brucei* the FP is essential for sur-
63 vival and this has been demonstrated through studies of an FP-linked cytoskeleton component
64 called the flagellar pocket collar (FPC). The FPC is a cytoskeletal structure that circumvents the
65 neck of the FP at the site where the flagellum exits the cell (13, 20–26). The FPC forms a cytoskele-
66 tal boundary or interface at the site of contact between the pellicular, flagellar and FP membranes

67 (13, 20, 23–26). To date, only a handful of FPC and FPC-associated proteins have been identified
68 and only two essential proteins have been characterized. The first is *TbBILBO1* (67kDa; 587aa)
69 which is the main protein component of the flagellar pocket collar (FPC), and the second is
70 *TbMORN1* (40.9kDa; 358aa) which is present in the Hook Complex (HC), a structure intimately
71 linked and immediately distal to the FPC, and is thought to indirectly play a role in facilitating pro-
72 tein entry into the cell. Two other FPC and FPC-associated proteins, *TbBILBO2* and *TbFPC4* re-
73 spectively, are *TbBILBO1* binding partners involved in a tripartite interaction (25, 27). Analysis of
74 *TbBILBO1* has demonstrated its uniqueness as a FPC component and it is indeed kinetoplastid-
75 specific. The N-terminus of *TbBILBO1* adopts a ubiquitin-like fold, followed by two calcium-
76 binding EF-hand domains (EFh1: amino acid residues 185–213 and EFh2 221–249). These domains
77 are followed by a large coiled-coil domain (CC, amino acids 263-566) and a C-terminal leucine
78 zipper (LZ, amino acid residues from 534–578) that are respectively involved in dimerization and
79 polymerization (14, 21, 22, 26). RNA interference (RNAi)-mediated knock-down of *TbBILBO1* in
80 the cultured, insect procyclic form (PCF) parasites prevents FPC and FP biogenesis, induces the
81 aberrant repositioning of the new flagellum (detached from the cell body along its length), and re-
82 sults in parasite cell death. Knock-down of *TbBILBO1* in the mammalian bloodstream form (BSF)
83 is rapidly lethal (14). The FPC is also intimately associated with the MtQ; a subset of specialized
84 microtubules that originate near the basal bodies of the flagellum and grow very close to, if not
85 through, the FPC (71, 72). Previous published work has identified binding of *TbMORN1* and
86 *TbSPEF1* (a microtubule binding and bundling protein) onto detergent and salt-extracted MtQ (20,
87 25, 73). Prior to those studies, our anti-*TbBILBO1* (IgM) antibody demonstrated both an FPC and a
88 minor MtQ signal. In considering the next steps of FPC analysis we decided to search for novel,
89 easily modifiable, molecular and immunological tools to study BILBO1. Subsequently, we decided
90 to raise nanobodies to purified *TbBILBO1* protein.

91

92 Nanobodies are derived from antibodies, more precisely, a specific class of heavy chain only anti-
93 bodies (HCAb) found naturally in Camelidae (alpacas, camels, llamas and vicunas) and also in
94 Elasmobranchs (cartilaginous fish - sharks and rays) (31, 32). Nanobodies are recombinant anti-
95 body fragments derived from the antigen binding domain (variable domain, VHH) of heavy chain
96 antibodies (33, 34). They are much smaller than traditional antibodies being ~ 15kDa in mass (35-
97 37). The use of nanobodies is greatly expanding in cellular and molecular biology, diagnostics, and
98 medicine (38-44). Indeed in 2018, caplacizumab was approved as the first nanobody-based drug
99 (45, 46). Intrabodies (INb), cytoplasmic nanobodies, have many potential roles ranging from patho-
100 gen detection, treating osteoarthritis and killing tumour cells (47), as well as therapeutic use for
101 neurological disease, viral infections (HIV) and autoimmune disease (39, 42, 54-58). Numerous
102 studies have used nanobodies to characterize trypanosome proteins (40, 43, 53, 59-69) but to date,
103 only one nanobody has been developed against a trypanosome cytoskeleton protein, Nb392, target-
104 ing the paraflagellar rod protein (PFR1)(66).

105105

106 RNA interference (RNAi) has been used to greatly enhance knowledge of gene and consequently
107 protein function in living cells. However, RNAi can have several limitations, such as incomplete
108 knockdown of the target protein. Furthermore, the double-stranded RNA produced during RNAi has
109 a relatively short half-life compared to an intrabody. Intrabodies are nanobodies expressed cyto-
110 plasmically in the target cell, and have the benefit of having high antigen specificity, the ability to
111 recognize and bind to a structural epitope not accessible by conventional antibodies, and have po-
112 tential as tools for many biological systems (49, 49-53). One advantage of intrabodies is that they
113 act at a post-translation stage, therefore they can target a specific isoform or post-translational mod-
114 ification of a protein (78). Also, in case of essential or structural proteins, induction of the expres-
115 sion of INbs at a specific cell-cycle, life-cycle stage or point in organelle biogenesis may provide
116 very subtle and precise phenotypes. In this regard, nanobodies also have advantages over conven-
117 tional antibodies due to their smaller size, allowing access to cryptic epitopes, and ability to cross

118 the blood-brain barrier (70, 71). Conventional antibodies have a further disadvantage of multi-
119 epitope cross-reaction, a phenomenon exemplified by IgE in allergen cross-reaction, whereas,
120 nanobodies are, theoretically, single epitope specific (37, 38, 72).

121121

122 We show here that, our anti-*TbBILBO1* (1-110) rabbit polyclonal, purified Nb48 and intrabody 48
123 (INb48) all bind to the FPC and the MtQ. Importantly, we demonstrate that intrabodies raised
124 against *TbBILBO1* can have comparable effects to RNAi knock-down and we establish that anti-
125 *TbBILBO1* intrabody (INb48) identifies its target protein when expressed in a homologous mam-
126 malian system *in vitro* and within the cytoplasm of *T. brucei*. Our data illustrates, for the first time,
127 a functional anti-cytoskeletal intrabody in *T. brucei*, that is able to precisely target and bind to its
128 target protein epitope and block biogenesis of a cytoskeletal structure leading to rapid cell death.
129 This data supports the hypothesis that targeting minor, yet essential, cytoskeletal proteins is of con-
130 siderable merit in the search to understand parasite biology. The results also suggest that the use of
131 intrabodies might be useful in organisms that do not have RNAi machinery or to characterize the
132 cell biology of emerging pathogens, marine organisms, protists and the numerous, new model or-
133 ganisms such as those described by Faktorová *et al* (73).

134134

135 **Results**

136136

137 **Production of anti-*TbBILBO1* nanobodies**

138 Full-length histidine-tagged *TbBILBO1* protein was expressed in bacteria (74). Purified recombi-
139 nant protein was then used to immunize an alpaca to produce *TbBILBO1* targeting nanobodies by
140 the Nanobody Service Facility (NSF, VIB, Brussels). Seven different Nbs were identified following
141 phage display screening. These were assigned to three different groups based on their amino acid
142 sequences. It was hypothesized that Nbs in the same group would recognize the same epitope, but

143 their other characteristics such as affinity, potency, stability and expression yield, could be different.
144 We chose to focus on one nanobody from each group for our current studies: Nb48, Nb9, and Nb73.
145

146 **Nb48 as a functional tool for immunolabelling *Tb*BILBO1**

147 The Nbs were cloned in the pHENC6c vector in frame with a HA and Histidine tag (Nb::*HA::6His*)
148 allowing the secretion of the Nbs in the periplasm, their purification using metal affinity chromatog-
149 raphy, and detection (Supplementary Figure S1). Samples of non-induced (-) and induced bacteria
150 (+), pellet (P) and periplasmic extracts (Ex) were probed by western blot with anti-HA (Supplemen-
151 tary Figure S2A and B). For simplicity, the HA::*6His* tagged nanobodies are hereafter called Nb48,
152 Nb9 and Nb73 (with tags written in subscript). We tested purified Nb48::*HA::6His*, Nb9::*HA::6His* and
153 Nb73::*HA::6His* by using anti-HA for detection in immunofluorescence microscopy (IFA) on *T.*
154 *brucei* wild-type (WT) procyclics (PCF) detergent-extracted cells (cytoskeletons) (Figure 1). For
155 convenience, in Figure 1 and 2, the cells that are probed with purified nanobodies are labelled as
156 “Anti-Nb”, plus the relevant nanobody name. In these experiments purified Nb48::*HA::6His* labels
157 endogenous *Tb*BILBO1 at the FPC, as seen by co-localization with anti-*Tb*BILBO1 (polyclonal
158 antibody 1-110) (Figure 1A). Nb9::*HA::6His* does not label wild-type cytoskeletons expressing en-
159 dogenous *Tb*BILBO1 protein (Figure 1B) but does label *Tb*BILBO1 in cells that over-express
160 *Tb*BILBO1::*3cMyc* (Figure 1C). Importantly, Nb73::*HA::6His* was negative in our experiments and did
161 not label *Tb*BILBO1 in either endogenous (Figure 1D) or overexpressed levels of *Tb*BILBO1 (not
162 shown).

163 To exclude the possibility of cross-reaction between primary and or secondary antibodies in double
164 labelling protocols, Nb48::*HA::6His* and anti-*Tb*BILBO1 (1-110) were also used alone to probe cyto-
165 skeletons. In both cases the subsequent labelling was observed on the FPC and the microtubule
166 quartet, (MtQ) a subset of specialized microtubules that are in close proximity to the FPC, but with

167 unknown function (71, 72), (Figures 2A and B). Labelling with anti-*Tb*BILBO1 (rabbit polyclonal,
168 1-110) alone also clearly labelled the MtQ (Figure 2C). Co-localization was observed in double
169 labelling experiments with anti-*Tb*BILBO1 (1-110) and Nb48::*HA*::6His (Figures 1A and 2D). In
170 Figures 2A-D, the asterisks indicate the labelling of the MtQ. Purified Nb48::*HA*::6His and
171 Nb9::*HA*::6His both positively label full-length *Tb*BILBO1 protein from *T. brucei* whole cell extracts
172 in western blotting experiments (Figure 2E and F) as well as *Tb*BILBO1 truncated versions
173 (T3::*3cMyc*, aa 171-587 and T4::*3cMyc*, aa 251-587) (please also refer to the schematic in Figure 2G
174 for an overview of the truncations). Neither, Nb48::*HA*::6His nor Nb9::*HA*::6His labelled T1 or T2 in-
175 dicating that Nb48::*HA*::6His and Nb9::*HA*::6His bind to *Tb*BILBO1 in the region ranging from aa 251
176 to aa 587. Controls for IFA experiments in Figures 1 and 2 are presented in Supplementary Figure
177 S2C.

178 **Surface Plasmon Resonance confirms a strong binding affinity of Nb48 to *Tb*BILBO1**

179 To determine the equilibrium dissociation constant (K_D) of Nb48::*HA*::6His (group 1) and
180 Nb9::*HA*::6His (group 2) to *Tb*BILBO1, we used surface plasmon resonance (SPR) (Figures 2H and
181 I) (note: It was not possible to assess Nb73::*HA*::6His (group 3) using SPR due to the inconsistent
182 yield and impure production of this nanobody from bacteria). Sensor chips were coated with puri-
183 fied 6His::*Tb*BILBO1 by amine coupling and probed sequentially at increasing concentrations with
184 purified Nb9::*HA*::6His and Nb48::*HA*::6His. The Nb binding results are shown on the sensorgrams
185 (Figures 2H and I) respectively, and are from a titration data set of three concentrations of the nano-
186 bodies: 31.3nM, 125nM and 500nM. These results illustrate that Nb9::*HA*::6His and Nb48::*HA*::6His
187 bind to 6His::*Tb*BILBO1, but do not behave kinetically in the same way. The superposition of the
188 sensorgrams with the fitting curves validates the Langmuir 1:1 model of interaction for analyzing
189 them. Nb9::*HA*::6His displays faster rate constants than Nb48::*HA*::6His with Nb9::*HA*::6His $k_a=6.54 \times$

190 $10^6 \pm 0.27 \times 10^6 \text{ M}^{-1} \text{ s}^{-1}$ and $k_b=98.9 \times 10^{-3} \pm 0.09 \times 10^{-3} \text{ s}^{-1}$, and Nb48::HA::6His $k_a=1.74 \times 10^5 \pm$
191 $0.16 \times 10^5 \text{ M}^{-1} \text{ s}^{-1}$ and $k_b=1.52 \times 10^{-3} \pm 0.02 \times 10^{-3} \text{ s}^{-1}$. Because of a 100x fold slower rate of disso-
192 ciation and despite a 10x fold slower rate of association, Nb48::HA::6His displays the highest affinity
193 for 6xHis::TbBILBO1 with a K_D of $8.8 \pm 0.7 \text{ nM}$ compared to Nb9::HA::6His K_D of $15.2 \pm 0.7 \text{ nM}$.
194 These values confirm that Nb48::HA::6His has the highest affinity for 6xHis::TbBILBO1. Nb48 pro-
195 vided the best results as a tool by IFA, as a probe on western blot and binding to TbBILBO1 as
196 measured by SPR, we therefore decided to focus on Nb48 for further studies.

197197

198 **Anti-TbBILBO1 intrabodies bind to the FPC and the MtQ**

199 Previous studies using STimulated Emission Depletion microscopy (STED), a technique of switch-
200 ing off the fluorescence of dye molecules by stimulated emission using laser light) (75), and immu-
201 no-electron microscopy have illustrated that the anti-TbBILBO1 (1-110) rabbit polyclonal antibody
202 labelled both at the FPC and the MtQ (25). It is important to note that Gheiratmand *et al.*, 2013,
203 Esson *et al.*, 2012 and Albisetti 2017 *et al.*, have shown that TbSPEF1 (a microtubule binding and
204 bundling protein) and TbMORN1 are localized to the MtQ of flagella thus clearly indicating that
205 they remain attached to this structure after harsh extraction and indicating that labelling of the MtQ
206 is not artefactual (73, 20, 25). Given that TbBILBO1 and TbMORN1 are stable on isolated flagella,
207 we questioned whether the FPC could be probed *in vivo* in trypanosomes by intra-nanobody (INb)
208 targeting. Consequently, the DNA sequence encoding Nb48 plus a C-terminal 3cMyc tag was
209 cloned into a *T. brucei* expression vector allowing the tetracycline-inducible expression of the re-
210 combinant Intrabody48 (INb48::3cMyc). Isolated flagella derived from procyclic cells (PCF) express-
211 ing INb48::3cMyc for 12 hours were prepared for IFA and double labelled by probing with anti-
212 cMyc and anti-TbBILBO1 (1-110) showing co-localization of TbBILBO1 and INb48 (Figure 3A).
213 For convenience the use of INb48 is displayed in these figures as Anti-INB48 rather than indicating

214 the tag used on the intrabody. Immuno-electron microscopy was also carried out on flagella that
215 were double labelled using anti-cMyc and anti-*TbBILBO1* antibodies (Figure 3B). Both the IFA
216 and the electron micrographs of these experiments revealed that INb48::3cMyc colocalizes with anti-
217 *TbBILBO1* on the FPC, but also on the proximal region of the MtQ as described earlier in the IFA
218 studies shown in Figures 2A-D. We also carried out temporally shorter expression assay of
219 INb48::3cMyc which revealed that it is observed on the FPC and the MtQ at 3 hours post induction
220 (Supplementary Figure S2D). Since INb9 also localized with *TbBILBO1* on the FPC, it was also
221 tested at reduced expression time (6 hours) and was shown on the FPC and colocalized with anti-
222 *TbBILBO1* (Supplementary Figure S2E).

223 **The expression of anti-*TbBILBO1* intrabodies is cytotoxic in *T. brucei***

224 Because anti-*TbBILBO1* intrabodies co-localize with *TbBILBO1* on isolated flagella, we hypothe-
225 sized that INbs bind tightly to *TbBILBO1* and, as a consequence, may disturb FPC formation or
226 function. To test this hypothesis, we monitored the effect of expression of INb48::3cMyc in PCF *T.*
227 *brucei* using different concentrations of tetracycline (Figure 4A). Tetracycline concentrations of 0.1
228 ng/mL and 1ng/mL had no impact on cell growth when compared to the non-induced cells (-Tet; red
229 line). However, concentrations from 5ng/mL to 1 μ g/mL induced a rapid growth defect from 24
230 hours post induction (hpi), and cell death after 24hpi. The change in growth rates related to different
231 doses of tetracycline indicates that the lethality of INb48::3cMyc expression in PCF is dose depend-
232 ent.

233 Taking in account these results, we chose a tetracycline concentration of 1 μ g/mL as the standard
234 concentration for INb48::3cMyc, INb9::3cMyc and INb73::3cMyc induction. After induction of the ex-
235 pression of these three INbs in trypanosomes, daily samples were taken for cell counts (Figure 4B-
236 D) and western blot analysis (Figure 4E). Independent induction of each INb resulted in pheno-
237 types that ranged from rapid cell death from 24hpi for INb48::3cMyc, (Figure 4B), to a reduction in

238 cell growth rate for INb9::3cMyc (Figure 4C) or no change in growth rate for INb73::3cMyc (Figure
239 4D). Western blot analysis of INb expression is shown in (Figure 4E) and illustrates robust expres-
240 sion of all INbs at 24 hours post induction in trypanosomes. After 48hpi of intrabody expression,
241 the signals for INb48::3cMyc and INb9::3cMyc were lost and the signal for *TbBILBO1* and tubulin
242 control proteins show signs of degradation, indicating some degree of cell death in the population.
243 However, little or no degradation is observed in cells expressing INb73::3cMyc which, importantly,
244 showed no effect on cell growth.

245245

246 As a negative control an intrabody against Green Fluorescent Protein (INbGFP::3cMyc) was ex-
247 pressed in trypanosomes, and as expected, no cell growth defect or phenotype was observed despite
248 its strong expression and cytoplasmic localization (Supplementary Figure 3A-C). These data
249 demonstrate that expression of INb48::3cMyc and of INb9::3cMyc are lethal, with INb48::3cMyc show-
250 ing the strongest effect, whilst expression of INb73::3cMyc had no effect on cell growth. The data
251 also suggest that INb48::3cMyc and INb9::3cMyc bind to *TbBILBO1* *in vivo*, and somehow hinder its
252 function.

253253

254 **Intrabody 48 (INb48::3cMyc) binds to *TbBILBO1* and induces *TbBILBO1* RNAi knockdown** 255 **phenotypes**

256 Trypanosome cell cycle stages can be defined based on the arrangement and number of nuclei and
257 mitochondrial genome (kinetoplasts) present in the cell. In wild-type G1 PCF cells, the linear or-
258 ganization of kinetoplast (K), and the nucleus (N) is: kinetoplast followed by the nucleus (1K1N).
259 As the cell passes through the cell cycle the kinetoplast duplicates to form 2K1N cells, then mitosis
260 and nuclear duplication ensues to form 2K2N cells with a posterior new flagellum (NF) and a more
261 distal old flagellum (OF), followed by cytokinesis producing 1K1N mother and daughter cells. This

262 means that wild-type cells should never possess more than the 2K2N DNA complement (76).
263 RNAi knockdown of *TbBILBO1* in cultured PCF cells results in cell-cycle arrest at the 2K2N stage,
264 producing cells with elongated posterior ends, new flagella that were detached from the length of
265 the cell body, and inhibition of new FPC formation (13). We investigated further the localization of
266 INb48 and its effects on cell morphology when expressed in *T. brucei* (Figure 5). Figure 5A shows
267 non-induced (-Tet, NI), whereby the NI trypanosomes display the classic immunofluorescence sig-
268 nal for *TbBILBO1* with the annular labelling at the FPC and along the MtQ between the FPC and
269 the basal bodies (BB). After 24hpi of INb48::3cMyc (+ 24h) *TbBILBO1* RNAi-like morphological
270 phenotypes were observed where the new flagellum was detached from the length of the cell body
271 and cells demonstrated elongated posterior ends. In *TbBILBO1*RNAi knockdown experiments very
272 little BILBO1 protein was observed at the new flagellum and only low levels were observed at the
273 old flagellum (74, 77). However, when INb48::3cMyc is expressed, both INb48::3cMyc and
274 *TbBILBO1* were sometimes observed at the old FPC and also at the base of the detached new fla-
275 gellum (Figure 5B, asterisk). More importantly, rather than the classic annular and MtQ signals ob-
276 served after anti-*TbBILBO1* labelling, we observed both *TbBILBO1* and INb48::3cMyc signals ex-
277 tending along the cell (Figure 5B, merged inset). This result demonstrates that no new FPC was
278 formed after INb48::3cMyc expression leading to the *TbBILBO1* RNAi-like phenotype and im-
279 portantly, that INb48::3cMyc binding to *TbBILBO1* disturbs FPC formation.

280280

281 Because FPC biogenesis is hindered in INb48::3cMyc induced cells, we decided to investigate the
282 organization of the hook complex (HC), a structure intimately associated with the FPC, by immuno-
283 labelling of *TbMORN1* (78) in the background of INb48::3cMyc induced mutant cells. The HC is an
284 essential structure positioned distal to the FPC, forming a distinctive hook shape, and is considered
285 to be indirectly involved in the regulation of entry of molecules into the flagellar pocket (20, 78–
286 80). Figure 5C illustrates the normal location and hook-like shape of anti-*TbMORN1* labelling in

287 non-induced cells. However, at 24hpi of INb48::3cMyc expression, *TbMORN1* labelling is elongated
288 distally along the flagellum, and the hook shape is lost (Figure 5D). Importantly, little or weak
289 *TbMORN1* labelling is observed at the base of the new flagellum, suggesting that HC biogenesis is
290 also strongly affected in cells expressing INb48::3cMyc. A consistent observation in cells expressing
291 INb48::3cMyc was that the new flagellum was detached from the length of the cell body, *i.e.* only
292 attached at the base, an abnormal phenotype strongly resembling the *TbBILBO1* RNAi knockdown
293 phenotype (14). We further characterized the detached new flagellum phenotype by co-labelling
294 with anti-*TbPFR2* antibody (8). *TbPFR2* is a protein of the paraflagellar rod (PFR) that is present
295 alongside the axoneme of the flagellum of wild-type *T. brucei* (81) as shown in non-induced cells
296 (Figure 5E). In induced cells (24hpi), *TbPFR2* labelling was observed along the old flagellum and
297 the newly detached new flagellum (Figure 5F). In this cell, INb48::3cMyc was only observed at the
298 old FPC, indicating that a new flagellum and PFR was formed in the absence of the FPC. To inves-
299 tigate any effect of INb48::3cMyc expression on the basal bodies (BB), an antibody marker anti-
300 *TbBLD10* was used, which was raised against *TbBLD10*, an essential protein in pro-basal body
301 biogenesis (82). Figure 5G shows a non-induced *T. brucei* cell with the typical labelling of the ma-
302 ture and pro-basal bodies. At 24hpi of INb48::3cMyc, the labelling of both the pro- and mature basal
303 bodies of the mother and daughter flagella were unaffected (Figure 5H). We also checked a longer
304 INb48::3cMyc expression (48hpi) by IFA and demonstrate that cells are severely compromised. Cells
305 showed cell cycle disruption including the presence of multiple flagella (Supplementary Figure S3
306 D and E). Also, the *TbBILBO1* labelling revealed extended structures demonstrating that the shape
307 of the polymers formed by *TbBILBO1* were strongly affected and were unable to form the typical
308 annular FPC.

309309

310 The phenotypes induced after INb48::3cMyc expression in trypanosomes were observed in more de-
311 tail by transmission electron microscopy (TEM). TEM micrographs of thin sections through the FP
312 (*) of a wild-type cell (Figure 6A) illustrate that the flagellum passes through this structure and that
313 its transition zone is positioned within the FP lumen (black arrow). INb48::3cMyc expression for 24
314 hours revealed that many of the new flagella were formed in the absence of an FP (Figure 6B, black
315 arrowheads indicate the position where the FP should be formed), and the transition zone is now
316 external to the cell (black arrows). These cells also accumulated cytoplasmic vesicles (Figure 6C).
317 These abnormal features are typical of *TbBILBO1* RNAi knockdown phenotypes (14) indicating
318 that *TbBILBO1* function was indeed hampered by the expression of INb48::3cMyc. We isolated fla-
319 gella from INb48::3cMyc trypanosome cells at 24hpi (+Tet) and probed them with anti-cMyc (for
320 INb48::3cMyc) and anti-*TbBILBO1* or, in a separate experiment, anti-cMyc and anti-*TbMORN1*. The
321 flagella were prepared for negative staining and visualized by transmission electron microscopy
322 (TEM). The co-labelling of INb48::3cMyc with *TbBILBO1* or *TbMORN1* revealed that these latter
323 proteins co-localize on the MtQ (Figure 6D and E). *TbBILBO1* was located on the MtQ proximal to
324 the basal bodies (Figure 6D), whereas *TbMORN1* was primarily on the MtQ distal to the basal bod-
325 ies (Figures 6E); it should be noted that *TbMORN1* was previously shown on the MtQ by Esson *et*
326 *al.*, (20) and Albisetti *et al.*, 2017 (25). Interestingly, however, the typical annular FPC structure is
327 absent in INb48::3cMyc induced trypanosomes, explaining the detached flagellum phenotype. In Fig-
328 ure 6D, INb48::3cMyc (arrowheads) is present alongside *TbBILBO1* (arrows) extending from the
329 basal bodies on the MtQ to the location where the FPC should be present. Figure 6E shows
330 *TbMORN1* labelling and shows in more detail that in the presence of INb48::3cMyc (arrowheads) it
331 is observed on the MtQ (arrows) extending in a linear fashion proximally along the flagellum but
332 not distally. These data demonstrate that the FPC and HC are structurally perturbed by the expres-
333 sion of INb48::3cMyc in *T. brucei*.

335 Expression of INb48::3cMyc disrupts the cell cycle in PCF *T. brucei*

336 The linear organization of kinetoplasts and nuclei in INb48::3cMyc expressing cells and morphologi-
337 cal phenotypes were analyzed at different time-points (Figure 7A). The percentage of non-induced
338 (-Tet) cell cycle stages were 74.4% in the 1K1N stage (blue bars), 13.9% in the 2K1N stage, and
339 9.4% in the 2K2N as previously published (14). A change was observed in trypanosomes expressing
340 INb48::3cMyc for 12 hours (+Tet 12h), with a reduction in 1K1N cells and an increase in 2K1N and
341 2K2N cells. There was also the appearance of abnormal K/N phenotypes such as 1K2N (1.5%)
342 when the nucleus had divided before the kinetoplast and cells with other abnormal K/N ratios in-
343 cluding cells with more than 2K and/or 2N annotated XKXN (1.6%). As previously mentioned,
344 when INb48::3cMyc is expressed in trypanosome cells, they exhibit detached flagella (18.3%). After
345 24hpi (+Tet 24h), this profile continued to augment with a further reduction in 1K1N (44.20%) and
346 a further increase in 2K2N cells (27.5%). Additionally, the number of 1K2N (abnormal) cells in-
347 creased to 4.3% and 5.9% of the population showed XKXN phenotype. Finally, the number of cells
348 with detached flagella had also increased to 35.4%. INb48::3cMyc expressing cells in the 2K2N
349 stage were further investigated and categorized according to linear organization of K and N from
350 posterior to anterior orientation (Figure 7B). For non-induced cells (-Tet), most 2K2N trypano-
351 somes had the normal KNKN organization with both flagella attached along the cell body (green
352 bar). At 12hpi, the number of normal 2K2N population has decreased (from 93.5 to 45.8%) with
353 the appearance of RNAi *TbBILBO1* knockdown-like 2K2N cells. 36.44% of the +Tet 12h total
354 2K2N population had detached flagella and an extended posterior end, which also included 15.8%
355 with a K_NKN organization (here the underscore refers to an extended end, - orange bar). 13.1% of
356 the abnormal population had a K_KNN kinetoplast organization (red bar) and 7.6% had a poorly
357 segregated nuclei K_NKN* (yellow bar). The other 2K2N population 17.7% (blue bar) included
358 cells that appeared normal in kinetoplast and nuclear organization KNKN but with detached flagel-

359 la, and cells with oddly misplaced kinetoplast (KKNN) with detached flagella. At 24hpi (+Tet 24h),
360 the proportion of 2K2N “normal-like” population was significantly reduced to 20.3% at the expense
361 of abnormal cells mentioned above. The rest of the abnormal cells possessed a detached new flagel-
362 lum which were distributed over a number of arrangements of K and N plus an extended posterior
363 end K_KNN (red bar), K_NKN (orange bar) and K_NKN* (yellow bar) or without extended poste-
364 rior ends (blue bar). These abnormal phenotypes are a clear indication of disruption of the cell cy-
365 cle. As with RNAi knockdown of *TbBILBO1*, it appears that there is a general cell cycle arrest at
366 the 2K2N stage, indicating the cells cannot undergo division. Overall, this indicates that the DNA
367 containing structures of the cell were able to divide and indeed separate (albeit imperfectly in some
368 cases), but the trypanosome cell itself was unable to undergo cytokinesis. With regards to these cell
369 cycle counts, similar findings were observed with RNAi knockdown of *TbBILBO1* (14), suggesting
370 that the crucial steps and structures required for cytokinesis, were impaired after INb48::3cMyc ex-
371 pression. Taken together, this data shows that INb48 targeting of *TbBILBO1* can be as effective as
372 RNAi knockdown.

373373

374 **Heterologous expression of *TbBILBO1* and INb48**

375 Expression of full-length and truncated forms of *TbBILBO1* in a U-2 OS heterologous system has
376 been published previously (23). In summary, that work had demonstrated that expression of full-
377 length *TbBILBO1* in mammalian cells induces the formation of linear polymers with comma and
378 globular shaped termini. To determine if Nb48 can bind to *TbBILBO1* as an antibody probe in this
379 heterologous system, we expressed full-length *TbBILBO1* in U-2 OS cells and probed detergent-
380 extracted cells with the purified Nb48 (Nb48::HA::6His) and with anti-*TbBILBO1* (1-110) (Figure
381 8B). Non-transfected, extracted U-2 OS cells were probed with anti-*TbBILBO1* (1-110) and
382 Nb48::HA::6His, and showed a negative signal (Figure 8A). When full-length *TbBILBO1* was ex-
383 pressed it induced the formation of long *BILBO1* polymers that were co-labelled with
384 Nb48::HA::6His and anti-*TbBILBO1* (1-110), (Figure 8B). *TbBILBO1* possesses two canonical cal-

385 cium-binding EF-hand domains; 1 and 2. Mutation of EF-hand domain 1 alone, or both EF-hands
386 together prevented the formation of linear polymers, however mutation of EF-hand domain 2 alone
387 (Mut2 EF-hand) resulted in the formation of helical polymers (23). We therefore used Mut2 EF-
388 hand to test for co-labelling with Nb48. Excellent co-labelling was observed when the Mut2 EF-
389 hand was expressed: the helical polymers of the mutated BILBO1 co-label with Nb48::HA::6His
390 (Figure 8C), suggesting that mutating the calcium-binding site, and preventing calcium binding,
391 does not affect Nb48 binding. We next expressed the *Tb*BILBO1 truncations T1, T2, T3, T4 (refer
392 to Figure 2G) in U-2 OS cells and used the previously anti-*Tb*BILBO1 monoclonal IgM antibody to
393 label T3 and T4 constructs (23). Previous studies had shown that *Tb*BILBO1 truncations T1 (aa1-
394 170) and T2 (aa1-250) are soluble in U-2 OS cells and do not form polymers (23). No signal was
395 observed when these extracted cells were probed by anti-*Tb*BILBO1 (1-110), furthermore no
396 Nb48::HA::6His signal was observed (Figures 8D and E). Truncations T3 (aa171-587) and T4
397 (aa251-587), however, form long polymers when expressed in U2-OS cells and, as with FL poly-
398 mers, these were positively co-labelled when probed with *Tb*BILBO1 and Nb48::HA::6His (Figures
399 8F and G). As such, this suggest that the Nb48 epitope lies between the amino acids 251-587. These
400 results illustrate that as a specific nanobody probe, Nb48::HA::6His, in a heterologous environment,
401 performed equally to a rabbit polyclonal antibody (anti-*Tb*BILBO1 1-110) and to anti-*Tb*BILBO1
402 IgM.

403403

404 To determine if INb48 can bind to *Tb*BILBO1 in the U-2 OS heterologous system and influence
405 polymerization, we co-expressed INb48::3HA with full-length *Tb*BILBO1 (FL), Mut2 EF-hand, or
406 truncated forms of *Tb*BILBO1. Expression of INb48::3HA alone produces a cytoplasmic signal in
407 whole cell preparations (Figure 8H), that was eliminated after detergent extraction (Figure 8I),
408 demonstrating that INb48::3HA does not bind to any cytoskeletal structure in U-2 OS cells, and does
409 not form polymers. When INb48::3HA was co-expressed with FL-*Tb*BILBO1, and cells detergent-

410 extracted, a strong co-localisation was observed between the *TbBILBO1* signal and that of
411 *INb48::3HA*, demonstrating that *INb48::3HA* was expressed, and binds to *TbBILBO1*, *in vivo*, in ex-
412 tracted conditions (Figure 8J and K). Importantly, however, the typical polymer structures that
413 *TbBILBO1* normally forms in U-2 OS cells (refer to Figure 8B) were absent. Instead, dense com-
414 pacted structures, attached to thin minor polymers were formed. Similar dense structures were ob-
415 served when Mut2-EFh was co-expressed with *INb48::3HA*, indicating that the EF hand domain 2
416 mutation (which prevents calcium binding) did not influence binding of *INb48::3HA* to *TbBILBO1*
417 (Figure 8L). This data indicates that binding of *INb48::3HA* to *TbBILBO1* modifies and reduces
418 linear polymerization in this environment.

419419

420 When *INb48::3HA* was co-expressed with T1 and with T2 (both have been demonstrated to be cyto-
421 plasmic in non-extracted cells) (23), a cytoplasmic signal was observed (Figures 8M and N). In con-
422 trast to the long, linear, polymers observed when T3 alone is expressed (Figure 8F), co-expression
423 of T3 and *INb48::3HA* induced dense globular structures (Figure 8O) similar to the observations
424 made when *INb48::3HA* was co-expressed with FL-*TbBILBO1* (Figures 8K) or Mut2-EFh (Figure
425 8L). Co-expression of *INb48::3HA* with T4 resulted in long polymers similar, but not identical, to
426 expression of T4 alone (as observed in Figure 8G). Instead, the *INb48::3HA* bound T4 polymers
427 were associated with many small, detergent insoluble, network-forming, polymers (Figure 8P),
428 which were never observed in T4 only expression as previously described (14) and suggests that
429 binding of *INb48::3HA* to T4 modifies normal polymerization. Taken together these data suggest a
430 critical disturbance by *INb48* in *TbBILBO1* polymer organization when co-expressed in a heterolo-
431 gous mammalian system. IFA controls for *INb48::3HA* and *TbBILBO1* expression in U-2 OS cells
432 alone and together can be found in Supplementary Figure S4 A-D demonstrating a lack of labeling
433 when no primary antibodies were used. Supplementary Figure S5 A-E shows the control intra-

434 nanobody against GFP (INbGFP) expressed in U-2 OS cells exhibiting a cytoplasmic signal which
435 was extracted in cytoskeleton preparations and did not co-localize or bind to *TbBILBO1* polymers
436 or any other structure. Negative and no primary antibody controls are also shown.

437437

438 Discussion

439 Nanobodies are rapidly being developed, not only as revolutionary therapeutics but also as biologi-
440 cal tools. In mammalian cells they have been used to assess protein function intracellularly (intra-
441 bodies), explore protein-protein interactions and as protein inhibitors (42, 83). Nanobodies have
442 been used in a number of experiments associated with trypanosomes including the potential of
443 nanobodies as diagnostic tools, in experimental therapy, and as trypanolytic agents (40, 54, 56, 58,
444 60–64, 84, 85). However, intrabodies have not been used to target the trypanosome cytoskeleton
445 intracellularly as a knockdown tool. This study shows that Nb48 proved to be an excellent tool for
446 detecting its trypanosomatid target antigen *TbBILBO1* by western blotting and by immunofluores-
447 cence (IFA) on fixed trypanosomes and immuno-electron microscopy. Further, when expressed as
448 an intrabody, INb48 targeted specifically *TbBILBO1* and functioned to disrupt the function of this
449 essential cytoskeletal protein.

450 The difference in the IFA behavior between Nb48 and Nb9 may be explained by their CDR3 se-
451 quences. If we consider that the two target epitopes are clearly different then this can, in part, ex-
452 plain a difference in detection by IFA. This would also suggest that binding of Nb48 to its BILBO1
453 epitope is possible under the, *in vivo*, native, BILBO1 expression levels within the FPC, whereas
454 binding of Nb9 is impaired due the possible presence of BILBO1 partner proteins that could partial-
455 ly shield the epitope or because the epitope is not fully exposed. Over-expression of BILBO1
456 would most probably produce and expose much more unshielded and/or accessible BILBO1 epitope
457 allowing Nb9 to bind. This would also explain why Nb9 was initially selected using ELISA assays
458 since the selection protocol was based on the use of purified, denatured recombinant BILBO1.

459 *INb48 modifies TbBILBO1 polymers in U-2 OS cells and in T. brucei*

460 Nb48 and INb9 both bind to the T4 domain of *TbBILBO1* (aa 251-587) demonstrating that they
461 recognize the same epitope *in vitro* and *in vivo*. Binding of INb48 to *TbBILBO1* in U-2 OS cells
462 modifies polymer structure and induced condensed structures (Figure 8J and K) compared to the
463 long, comma or annular shaped polymers that are normally observed (23). INb48 binds to the do-
464 main of *TbBILBO1* that includes the CCD and the LZ domains both involved in protein-protein
465 interaction, and importantly, the CCD domain is required for dimerization and the LZ for polymeri-
466 zation (22, 23). Based on the structures observed in the U-2 OS cells, both dimerization and
467 polymerization occur, but it is difficult to speculate on how INb48 affects the polymers. However,
468 one could expect the same effect in parasites, resulting in alteration in FPC formation. Indeed, the
469 expression of INb48 in *T. brucei* led to perturbation of the structure of the FPC and the HC, as seen
470 by IFA and iEM labelling of *TbBILBO1* and *TbMORN1* respectively. Interestingly, INb48 labelled
471 strongly the MtQ and the typical annular FPC structure and “hook and shank” aspect of the HC was
472 not observed in many salt-extracted flagella in iEM experiments. Also, IFA experiments demon-
473 strated (*via* the elongated structures labelled with an anti-BILBO1 polyclonal), that INb48 affects
474 the biogenesis of the FPC. This suggests that *TbBILBO1* and *TbMORN1* traffic along the MtQ.

475475

476 *INb48 induces BILBO1-RNAi knockdown-like phenotypes*

477 The perturbations of *TbBILBO1* assembly by INb48 leads to RNAi knock-down-like phenotypes
478 and this included the endomembrane system (14). Although membrane trafficking was affected by
479 INb48 expression, it does not have membrane targeting or retention signals, which are sometimes
480 used on INbs (86). This suggests that the accumulation of intracellular vesicles following INb48
481 expression (Figure 6) are due to disruption in endo-/exocytosis and is a downstream consequence of
482 the disturbance of the flagellar pocket and the HC. After 24h of INb48 induction there is no INb48
483 or BILBO1 protein degradation and the BILBO1 RNAi-like phenotypes are apparent, but at 48h
484 induction there is considerable protein degradation probably due to cell lysis. INb48 binding to

485 BILBO1 might result in BILBO1 sequestration, which could lead to intense disruption of the FP
486 and that at some point this induces cell lysis. It is also possible that the intrabody binds to BILBO1
487 that has already been incorporated into the FPC, but does not disrupt its function. If the intrabody is
488 only able to capture free BILBO1 the difference in effect on free *vs* FPC-incorporated BILBO1
489 could explain the delay in the phenotype. In this context, it is noteworthy that we also observed
490 dramatic changes in BILBO1 polymers when co-expressed with INb48 in U2-OS cells. The binding
491 of INb48 to newly forming BILBO1 polymers could prevent correct FPC formation by inducing
492 malformation of the growing BILBO1 polymers. Indeed, figures 5B and D (and Supplementary
493 Figure S3 D and E) illustrate the formation of unusual, BILBO1 positive, linear polymers, when
494 INb48 was expressed in trypanosomes, instead of the annular polymers normally present in a wild-
495 type FPC. We are currently investigating the knockdown effect in more detail and also the traffick-
496 ing of FPC proteins to the FPC, to ascertain whether the MtQ is implicated. This may also answer,
497 in part, the question of how the FPC, a flagellum-associated complex of proteins, is built.

498498

499 In conclusion, we induced a BILBO1 RNAi phenotype not by knocking down protein expression
500 but rather by preventing protein function. This indicates that an intrabody-induced, protein binding
501 approach can prevent the formation of a new FPC most likely even in presence of BILBO1 interact-
502 ing proteins. This would indeed suggest that BILBO1 is the main protein performer in FPC biogen-
503 esis. Therefore, our data support the hypothesis that targeting minor, yet essential, cytoskeletal pro-
504 teins is of considerable merit in the search to understand parasite biology. Intrabodies would be use-
505 ful in organisms that do not have RNAi machinery and to characterize the biology of emerging
506 pathogens, newly discovered protists and new model organisms (73). As a consequence, the data
507 presented here demonstrates, for the first time, the use of a functional, tractable, anti-cytoskeletal
508 intrabody in *T. brucei*, that is able to precisely target and bind to its target epitope and induce dis-
509 ruption of a cytoskeletal structure leading to rapid cell death.

510510

512 **Materials and Methods**

513513

514 **Ethics statement**

515 The alpaca immunization was carried out by Nanobody Service Facility, VIB Rijvisschestraat 120,
516 9052, Belgium and was approved by the Ethical Committee for Animal Experiments of the Vrije
517 Universiteit Brussel (VUB), Brussels, Belgium.

518518

519 **Alpaca immunization and Nb library construction**

520 HIS-tagged, full-length *T. b. brucei* BILBO1 protein ($_{6\text{HIS}}::Tb\text{BILBO1}$) was expressed in bacteria,
521 purified in urea on Ni-NTA resin by affinity column purification, as described in (25), and sent to
522 Nanobody Service Facility (NSF, VIB, Brussels). The nanobody library was constructed as de-
523 scribed by NSF-VIB (Nanobody Service Facility, Belgium) and produced 2×10^8 independent trans-
524 formants that were subjected to two rounds of panning, performed on solid-phase coated full-length
525 *TbBILBO1* antigen (10 μg /well). Ninety-five colonies from round two were randomly selected and
526 analyzed by ELISA for the presence of antigen-specific Nbs in their periplasmic extracts. Thirty-
527 four colonies scored positive, representing seven different Nbs from three different groups based on
528 their gene sequences: Nbs in each group have very similar sequence data. The Nb genes were
529 cloned into a pMECS vector containing a secretion PelB leader signal sequence at the N-terminus, a
530 hemagglutinin A (HA) tag and a hexa-histidine (His) tag at the C-terminus, for purification and im-
531 munodetection. These vectors were transformed into TG1 *E. coli* and stored at -80°C .

532532

533533

534 **Nanobody cloning and bacterial expression**

535535

536 Nbs were sub-cloned from pMECS to pHEN6c vector as follows: TG1 *E. coli* harboring the Nbs,
537 were grown overnight on solid agar + ampicillin (100 μg /mL). The Nb genes were amplified by
538 PCR directly on colonies using specific primers A6E (5'GAT GTG CAG CTG CAG GAG TCT

539 GGR GGA GG 3') and PMCF (5' CTA GTG CGG CCG CTG AGG AGA CGG TGA CCT GGG T
540 3'). PCR fragments were digested with *Pst*I and *Bst*II then ligated into the pHEN6c vector har-
541 boured in XL1 blue *E. coli* and stored at -80°C. For expression and purification, WK6 *E. coli* were
542 transformed with pHEN6c harbouring the Nb. PCR on transformed colonies, using M13R (5' TCA
543 CAC AGG AAA CAG CTA TGA C 3') and PMCF (5' CTA GTG CGG CCG CTG AGG AGA CGG
544 TGA CCT GGG T 3') confirmed the Nb insert. *Tb*BILBO1, *Tb*BILBO1 EF-hand domain mutant 2
545 and *Tb*BILBO1 truncations T1, T2, T3 and T4 were expressed in the heterologous mammalian sys-
546 tem, U2-OS, by using pCDNA3 vector as described in (23). Nb48 sequence was cloned into the
547 pcDNA3.1 C-terminus tag 3HA vector (derived from pCDNA3.1 Invitrogen) between *Nhe*I-*Xho*I
548 restriction sites and expressed transiently as an intrabody, INb48::3HA.

549549

550 **Intra-nanobody expression in Trypanosoma**

551 The Nb inserts were digested out from pHEN6c with *Hind*III and *Nde*I and cloned into *Hind*III and
552 *Nde*I digested pLew100-3cMyc (86). Plasmid sequences were confirmed by DNA sequencing.

553553

554 **Nanobody expression and purification**

555 Freshly transformed WK6 with pHEN6c-Nb vectors were inoculated into 10mL LB + ampicillin
556 (100µg/mL) + 1% glucose and incubated overnight at 37°C, shaking at 250 rpm. Terrific broth (TB)
557 medium was prepared for Nb expression (2.3g/L KH₂ PO₄, 16.4g/L K₂ HPO₄.3H₂O, 12g/L Tryp-
558 tone, 24g/L Yeast extract, 4% glycerol). One mL of culture was added to 330mL TB + 100µg/mL
559 ampicillin, 2mM MgCl₂ and 0.1% glucose, incubated at 37°C, shaking 250 rpm, until a mid-log
560 phase of growth OD₆₀₀ of 0.6-0.9 was reached. Nb expression was induced with 1mM Isopropyl β-
561 D-1-thiogalacto-pyranoside (IPTG). The culture was incubated for 17 hours at 28°C with shaking.
562 Nb was extracted from the periplasm as follows. Cultures were centrifuged for 16 minutes at 4,500
563 x g. The pellet was re-suspended in 4mL of TES (0.2M Tris pH8.0, 0.5mM EDTA, 0.5M sucrose),
564 then shaken for 1 hour on ice at 110 rpm. Four mL of TES/4 (TES diluted 1:4 in water) was added

565 and further incubated on ice for 1 hour with shaking, then centrifuged for 60 minutes at 4,500 x g at
566 4°C to releases the contents of the periplasmic space (87). The supernatant contains the periplasmic
567 extract with Nb. A control periplasmic extraction was performed using the same procedure as
568 above, without the Nb insert in the vector.

569569

570 The periplasmic extract was filtered on 0.45 µm, and loaded onto a HisTrapTMFF column (GE
571 Healthcare) pre-equilibrated with running buffer (PBS, 20mM imidazole, 10% glycerol, protease
572 Inhibitor Cocktail Set III Calbiochem, Ref. 539134-1 at 1:10,000 dilution). The column was washed
573 with five column volumes (CV) of lysis running buffer and bound protein was eluted by 500 mM
574 imidazole/running buffer with 10 CV. Elutions containing the highest concentration of purified
575 nanobody were pooled and dialysed against 1xPBS + 20% glycerol using Slide-A-LyzerTM (Thermo
576 Scientific B2162132) and stored in 1xPBS + 20% glycerol. To verify the presence of Nb in purified
577 elutions, 10µL from each elution was run on 15% SDS-PAGE gel stained with Coomassie Brilliant
578 Blue (Instant BlueTM Expedeon Ltd). Proteins from a second identically loaded gel were transferred
579 to PVDF membrane using a semi-dry transfer method (BIORAD) and a western blot was performed
580 using anti-HIS (Sigma H-1029, mouse, 1:3000) and anti-HA (Biolegend MMS-101R or, Santa-Cruz
581 7392, 1:1000) antibodies to detect the Nb, followed by anti-mouse HRP conjugated (Jackson, 115-
582 035-044, 1:10,000 or, Jackson, 515-035-062 1:1000).

583

584 **Surface Plasmon Resonance Assays**

585 Surface plasmon resonance (SPR) was used to measure the binding affinity of the nanobodies to
586 *TbBILBO1* purified protein, the benefits being it is measured in real-time and is label-free. All solu-
587 tions and buffers used were filtered and degassed. The experiments were performed at 25°C using a
588 BiacoreTM T200 instrument (GE Healthcare Life Sciences, Uppsala, Sweden) flowed with EP+
589 buffer (10mM HEPES, pH 7.4, 150mM NaCl, 3mM EDTA, 0.05% Tween-20) from the manufac-
590 turer as running buffer. For *TbBILBO1* expression, _{6His::}*TbBILBO1* protein was overexpressed in

591 bacteria, soluble supernatant purified on Ni-NTA resin as describe in (13). Briefly, the cells were
592 grown at 37°C in Luria–Bertani (LB) medium containing 50µg/mL kanamycin to OD₆₀₀ 0.6. The
593 cells were cold-shocked on ice for 30 minutes and induced with of 1mM of IPTG for 2 hours at
594 16°C. After centrifugation, the cell pellet was lysed by sonication in lysis buffer (2mM Tris–HCl pH
595 7.4, 0.5M NaCl, 20mM imidazole, 10% glycerol, Protease Inhibitor Cocktail Set III Calbiochem,
596 1:10,000) and centrifuged (10,000g, 30 minutes, 4°C) to remove cell debris. The supernatant was
597 filtered at 0.45µm, and loaded onto a HisTrapTMFF column (GE Healthcare) pre-equilibrated with
598 the same lysis buffer. The column was washed with 5 column volumes (CV) of lysis buffer and
599 bound protein was eluted by 500mM imidazole with 10 CV in lysis buffer. *Tb*BILBO1 fractions
600 were pooled and dialyzed against PBS, 10% glycerol and concentration was measured using Ther-
601 mo ScientificTM NanoDrop 2000. *Tb*BILBO1, prepared at 50µg/mL in 10mM sodium acetate buffer,
602 pH 7, was immobilized on a one flow cell of a CM5 sensor chip (GE-Healthcare, lot no 10266084)
603 by amine coupling as indicated by the manufacturer and the protein solution was injected for 11
604 minutes; 2973 resonance units (RU) of protein were immobilized. One flow cell was left blank for
605 double-referencing of the sensorgrams. The nanobodies were dialyzed against the EP+ running
606 buffer and were injected over the target by Single-Cycle Kinetics (SCK). This method consists of
607 injecting the partner sequentially at increasing concentration without a regeneration step between
608 each concentration injected. Protein concentrations were determined using a Thermofisher
609 NanodropTM One spectrophotometer (Ozyme) and were injected over the target by Single-Cycle
610 Kinetics (SCK) (89, 90). The surface was regenerated after each SCK cycle with two 1 minute puls-
611 es of 10mM glycine-HCl pH 2.1. The sensorgrams were analyzed with Biacore T200-v2.0 evalua-
612 tion software using a Langmuir 1:1 model of interaction to determine the association (k_a) and disso-
613 ciations (k_b) rate constants. A regeneration test was performed using 10mM glycine-HCl pH 2.1
614 (GE healthcare), 10mM glycine HCl pH2.1, at 30µg/min for 30 seconds with *Tb*BILBO1 alone to
615 ensure no loss of signal. The dissociation equilibrium constant, K_D , was calculated as k_b/k_a . The

616 values shown are the average and standard deviation of three independent experiments with samples
617 injected in duplicate.

618618

619 **Trypanosome cell lines, culture and transfection**

620 Procyclic (PCF) cell line Tb427 29.13 *Trypanosoma brucei brucei* (86) was grown in SDM-79 me-
621 dium (GE Healthcare, G3344-3005) pH7.4 supplemented with 2 mg/mL hemin (Sigma Aldrich, H-
622 5533), 10% fetal bovine serum complement deactivated at 56°C for 30 minutes (FBS; Gibco,
623 11573397;) and incubated at 27°C. Selection antibiotics hygromycin (25µg/mL) and neomycin
624 (10µg/mL) were added to the media to maintain the plasmid vectors pLew29 and pLew13 (86). For
625 transfection, the pLew100_Nb_3cMyc plasmids were linearized with *NotI*, then concentrated and
626 purified by ethanol precipitation. Laboratory cell lines PCF Tb427 29.13 were grown to 5-10x10⁶
627 cells/mL, then 3x10⁶ cells were electro-transfected with 10µg of plasmid using the program X-001
628 of the Nucleofector®II, AMAXA apparatus (Biosystems) as described in reference (88) with the
629 transfection buffer described in (91). After transfection, clones were obtained by serial dilution and
630 maintained in logarithmic phase growth at 2x10⁶ cells/mL . Selection antibiotics hygromycin
631 (25µg/mL) and neomycin (10µg/mL) were added to the media to maintain the laboratory cell lines
632 Tb427 29-13 (procyclic forms, PCF). Phleomycin (5µg/mL) was added to the media of transfected
633 cells to select for those harboring the pLew100-3cMyc vector and the Nb gene. Expression of Nb in
634 the parasites (intrabody) was induced with tetracycline at 0.1ng/mL - 1µg/mL tetracycline. Growth
635 curves representing logarithmic number of cells were calculated by counting the number of cells
636 every 24 hours using Mallassez counting chamber slides. Error bars represent SEM = standard error
637 of the mean.

638638

639 **Mammalian cell line culture and transfection**

640 U-2 OS cells (human bone osteosarcoma epithelial cells, ATCC Number: HTB-96) (88) were grown
641 in D-MEM Glutamax (Gibco) supplemented with final concentrations of 10% fetal calf serum

642 (Invitrogen), 100 units/mL of Penicillin (Invitrogen), and 0.100mg/L of Streptomycin (Invitrogen)
643 at 37°C plus 5% CO₂. Exponentially growing U-2 OS cells in 24 well plate with glass coverslips
644 were lipotransfected as described in (89) with 0.5µg of DNA using lipofectamine 2000 in OPTI-
645 MEM (Invitrogen) according to the manufacturer's instructions and processed for immunofluores-
646 cence 24 hours post-transfection.

647647

648 **Western blot analysis**

649 Trypanosomes were collected, centrifuged at 800 x g for 10 minutes, and washed in 1xPBS. For
650 whole cell samples, the number of trypanosomes to be loaded per well were calculated, then re-
651 suspended in protein sample buffer 2x, plus nuclease 250 IU/mL (Sigma Aldrich, Ref. E1014). The
652 samples were boiled at 100°C for 5 minutes then stored at -20°C until required. 15% SDS-PAGE
653 gels were prepared and samples loaded at 5x10⁶ WT PCF trypanosome cells, or PCF expressing
654 pLew100-Nb-3cMyc (induced with tetracycline 1µg/mL, 24 - 48 hours). For detection of Nb in bac-
655 terial periplasmic extract, 2x10⁸ bacterial cells or equivalent volume of periplasmic extract, flow
656 through or elution were loaded. Samples were separated according to manufacturer's recommenda-
657 tions then transferred in a semi-dry system (BIORAD Trans-Blot Semi-dry transfer cell
658 221BR54560) onto PVDF membrane and incubated with blocking solution (BS: 5% skimmed milk
659 powder, 0.2% Tween 20 in 1xTBS) for 60 minutes. For detection of intrabody, INb::3cMyc, expres-
660 sion in trypanosomes, an anti-cMyc antibody (Sigma, rabbit, C-3956) was diluted in blocking solu-
661 tion 1:1000 and incubated with the membranes overnight at 4°C. Membranes were washed in
662 1xTBS and then in BS before probing with anti-rabbit antibody conjugated to Horse Radish Peroxi-
663 dase (HRP) (1:10,000 in BS, Sigma, goat, A9169) for 60 minutes at RT. The following antibodies
664 were also used as primaries: anti-*Tb*BILBO1 aa1-110 (rabbit polyclonal, 1:1,000) (23); anti-
665 *Tb*Enolase (rabbit polyclonal, 1:25,000) (94), and anti-TAT1 (anti-Tubulin mouse monoclonal,
666 1:1,000) (95) were used as loading controls. A secondary anti-mouse HRP antibody was also used,
667 diluted 1:10,000 (Jackson, sheep, 515-035-062). Revelation was carried out using Image Quant

668 LAS 4000 (GE) or Chemidoc (Biorad). Purified Nbs were used as primary antibodies in western
669 blot assays to detect the presence of *Tb*BILBO1 in whole trypanosome cells. Whole cell extract of
670 5×10^6 WT PCF trypanosome cells, or PCF expressing *Tb*BILBO1-3cMyc, full-length or truncations
671 of *Tb*BILBO1 (T1, T2, T3, T4, induced with tetracycline $1 \mu\text{g}/\text{mL}$, 24 hours), were loaded on 12 or
672 15% SDS-PAGE. Western blots were carried out as described above and the purified Nb::3HA::6His
673 was used at a concentration of $10 \mu\text{g}/\text{mL}$ to probe the membranes. To detect purified nanobody, an
674 anti-HA (1:1000, Biolegend, 901513) or anti-HIS (1:10,000, Sigma H1029) was used, followed by
675 an anti-mouse HRP conjugated secondary (above).

676676

677 **Immunofluorescence assay (IFA)**

678 One mL of log-phase trypanosomes were collected, centrifuged for 5 minutes at $1000 \times g$, washed
679 in 1x PBS, then $20 \mu\text{L}$ was loaded onto poly-L-lysine 0.1% solution (P8920 Sigma-Aldrich) coated
680 slides for 4 minutes to adhere. Whole cells were fixed in methanol at -20°C for at least 60 minutes.
681 Cytoskeleton extraction was with 0.25% NP40 in PIPES buffer (100 mM PIPES pH 6.8, 1mM
682 MgCl_2) for 5 minutes, washed twice in PIPES buffer and cytoskeletons were fixed with 1% PFA or
683 methanol. Fixed trypanosomes were incubated with single or combination antibodies: anti-cMyc
684 (monoclonal antibody IgG1 9E10, 1:20) to detect expressed INb, anti-*Tb*BILBO1 (amino acids 1–
685 110, rabbit, 1517028 bleed 1 1:4000), anti-*Tb*MORN1 (rabbit 1:5000), anti-*Tb*PFR2 (rabbit 1:200),
686 anti-*Tb*BLD10 (rabbit 1:2000), for 60 minutes, washed twice in 1xPBS, then incubated with sec-
687 ondary antibodies: anti-mouse IgG FITC-conjugated (Jackson, 115-095-164), and anti-rabbit Alexa
688 fluor 594-conjugated (Invitrogen, A-11012). Kinetoplasts and nuclei were stained with $10 \mu\text{L}$ DAPI
689 ($10 \mu\text{g}/\text{mL}$) in 1xPBS for 2 minutes and slides were mounted with Slowfade® Gold antifade reagent
690 (Invitrogen, Molecular Probes). Images were acquired on a Zeiss Axioimager Z1 using MetaMorph
691 software and a Roper CoolSNAP HQ2 camera. For Nbs used as probes in IFA of fixed trypano-
692 somes, PCF *Tb*427 29.13 wild type (WT) and *Tb*427 29.13 pLew100-*Tb*BILBO1-3cMyc were fixed
693 (as above) incubated with Nb ($0.25 \text{mg}/\text{mL}$) for 1 hour, followed by anti-HA (Biolegend, 901513,

694 mouse) diluted 1:200. For co-labelling with *TbBILBO1*, anti-*TbBILBO1* (1-110) was used diluted
695 1:4000 in 1xPBS. Secondary antibodies were used with 1:100 dilution: anti-mouse FITC-
696 conjugated (Sigma, F2012), anti-rabbit Alexa fluor 594-conjugated (Invitrogen, A11012). For IFA
697 on U-2 OS cells, cells were fixed and processed as described in (23, 25). The primary antibodies
698 anti-*TbBILBO1* (1-110), 1:4000 dilution; anti-*TbBILBO1* (IgM) mouse monoclonal, 5F2B3, (14)
699 1:2 dilution; anti-HA epitope tag (mouse monoclonal, Biolegend, 1:1000); anti-HA (rabbit,
700 GeneTex GTX115044, 1:1000) were incubated for 1h in a dark moist chamber. After two 1 x PBS
701 washes, cells were incubated for 1 hour respectively with the secondary antibodies goat anti-rabbit
702 IgG (H+L) conjugated to Alexa fluor 594 (Molecular Probes A-11012, 1:400); goat anti-mouse IgM
703 conjugated to Alexa fluor 594 (Invitrogen, 1:400); goat anti-mouse whole molecule conjugated to
704 FITC (Sigma F-2012, 1:400); goat anti-rabbit IgG (H+L) conjugated to Alexa fluor 594 (Molecular
705 Probes A-11012, 1:400). Purified Nb48::*HA*::6His raised against *TbBILBO1* was used as a probe (10
706 µg/mL) and incubated for 1h in a dark moist chamber. After two PBS washes, cells were incubated
707 for 1 hour with the secondary antibody directed against the HA tag, anti-HA epitope tag (Biolegend,
708 1:1000) then washed twice in PBS and incubated 1 hour with the tertiary antibody goat anti-mouse
709 whole molecule conjugated to FITC (Sigma, 1:400). The intrabody anti-GFP nanobody 3 x HA-
710 tagged (INbGFP::*3HA*) was probed with anti-HA mouse IgG Biolegend, diluted 1:1000 in PBS FCS
711 10%, saponin 0.1% and probed with anti-mouse goat whole molecule FITC, Sigma, diluted 1:100 in
712 PBS FCS 10%, saponin 0.1%. The nuclei were stained with DAPI (0.25 µg/mL in PBS for 5
713 minutes). Slides were washed and mounted with Prolong (Molecular Probes S-36930). Images were
714 acquired on a Zeiss Imager Z1 microscope with Zeiss 63x objective (NA 1.4), using a Photometrics
715 Coolsnap HQ2 camera and Metamorph software (Molecular Devices), and processed with ImageJ
716 (NIH).

717

718 **Flagella preparation for IFA**

719 Ten mL of mid-log PCF cells were collected and washed once in 1xPBS for 5 minutes at 1000 x g
720 at RT. Cells were extracted with 1mL 1% NP40 in 100mM PIPES pH6.9, 1mM MgCl₂ for 7
721 minutes at RT to make cytoskeletons. Cytoskeletons were centrifuged for 10 minutes at 5,000 x g at
722 4°C and further extracted for 15-30 minutes on ice with 1% NP40 in 100mM PIPES buffer + 2mM
723 MgCl₂, containing 1M KCl. Flagella were centrifuged for 5 minutes at 5,000 x g at 4°C, the super-
724 natant was removed and flagella were resuspended in 500µL PIPES buffer. Flagella were washed
725 twice in 100mM PIPES buffer + 1mM MgCl₂ for 5 minutes 5000 x g at 4°C before being deposited
726 on poly-lysine coated slides and left to adhere for 5–10 minutes. The flagella were fixed at -20°C in
727 MeOH or in 3% PFA as described above.

728728

729 **Transmission Electron microscopy**

730 Ten mL of mid-log phase procyclic, *Tb427* 29.13 wild type (WT) cells, pLew100-Nb48-3cMyc,
731 (induced for 24h) were fixed, dehydrated and embedded, cut and stained as in (13) with the excep-
732 tion that tannic acid was omitted and cells were initially fixed in their culture medium by the addi-
733 tion of glutaraldehyde to a final concentration of 2.5% and paraformaldehyde at 3.7% for two hours
734 then pelleted at 1,000 x g and fixed for 2 hours in 2.5% glutaraldehyde in phosphate buffer pH 7.4.

735735

736 **Immuno-electron microscopy**

737 Ten mL of mid-log phase $\sim 5 \times 10^6$ /mL pLew100-Nb48-3cMyc cells were induced with 1µg/mL
738 tetracycline for 24 hours. Five mL of induced cells were harvested at 1,000 x g, for 5 minutes,
739 washed twice with PBS by centrifugation (1,000 x g) resuspended in 500µL of PBS. Freshly glow-
740 discharged, formvar and carbon-coated G2000-ni nickel grids (EMS) were floated on the droplets
741 and the cells allowed to adhere for 15 minutes. Grids were then moved onto a drop of 1% NP-40 in
742 PEME buffer (100 mM PIPES pH 6.8, 1 mM MgCl₂, 0.1mM EGTA) (5 min, RT), followed by in-
743 cubation on a 500µL drop of 1% NP-40, 1M KCl in PEME buffer for 15 minutes (3 x 5 minutes,
744 4°C). Flagella were washed twice (2 x 5 minutes) in PEME buffer at RT, equilibrated and blocked

745 on 50 μ L drops of 2% fish skin gelatin (Sigma-Aldrich G7041) or 0.5% BSA, 0.1% tween 20 in PBS,
746 incubated in 25 μ L of primary antibody diluted in blocking buffer (each primary antibody was used
747 either alone, or mixed with a second primary antibody), 1 hour at room temperature (RT). Anti-
748 cMyc IgG mouse monoclonal antibody, (9E10, purified, a kind gift from Pr. Klaus Ersfeld), was
749 diluted 1:10 or protein G purified/concentrated supernatant (diluted 1:50). Anti-*Tb*BILBO1 (1-110)
750 was diluted 1:200 or 1:400. Grids were blocked and incubated in secondary antibody for 1 hour at
751 RT (anti-mouse goat GMTA 5nm gold, and/or anti-rabbit goat 15nm gold GAR15, BBInternational-
752 al) 1:10 in 0.2% fish skin gelatin in PBS. Grids were blocked, and fixed in 2.5% glutaraldehyde in
753 0.2% fish skin gelatin in PBS. Samples were negatively stained with 1% aurothioglucose (Sigma-
754 Aldrich) (10 μ L for 30 seconds). Micrographs were taken on a Phillips Technai 12 transmission
755 electron microscope at 100 kV.

756756

757 **Acknowledgments**

758 We thank our lab members for insightful comments on the manuscript, Dr. Brooke Morriswood,
759 (University of Wurzburg, Germany) for the anti-*Tb*MORN1 antibody, Pr. Keith Gull (University of
760 Oxford, England) for the anti-TAT1 (anti-Tubulin) antibody, Dr. Zyin Li (University of Texas, USA)
761 for the anti-*Tb*BLD10 antibody, Pr. Klaus Ersfeld (University of Bayreuth, Germany) for the anti-
762 cMyc (9E10) antibody, Dr. Frédéric Bringaud, (University of Bordeaux, Bordeaux, France) for the
763 anti-Enolase antibody and Dr. Nicolas Biteau (University of Bordeaux, Bordeaux, France) for the
764 anti-*Tb*PFR2 rabbit polyclonal antibody. The Robinson lab acknowledges supported by the Centre
765 National de la Recherche Scientifique (CNRS, <https://www.cnrs.fr/>), and the Université de Bor-
766 deaux (<https://www.u-bordeaux.fr/>). CBR and MRR were supported by fellowships from the French
767 Ministry of Higher Education, Research and Innovation (<https://www.enseignementsup->
768 [recherche.gouv.fr/](https://www.enseignementsup-recherche.gouv.fr/)). We acknowledge funding from the Fondation pour le Recherche Médicale
769 (FRM, <https://www.frm.org/>) (FRM) grant number FDT202001010783 awarded to MRR. This
770 work was also supported by Laboratoire d'Excellence (<https://www.enseignementsup->

771 recherche.gouv.fr/cid51355/laboratoires-d-excellence.html) through the LabEx ParaFrap (grant
772 number ANR-11-LABX-0024) awarded to DRR.

773773

774 **References**

- 775 1. Diall O, Cecchi G, Wanda G, Argilés-Herrero R, Vreysen MJB, Cattoli G, Viljoen GJ, Mattioli
776 R, Bouyer J. 2017. Developing a Progressive Control Pathway for African Animal Trypanoso-
777 mosis. *Trends Parasitol* 33:499–509.
- 778 2. Simarro PP, Cecchi G, Franco JR, Paone M, Diarra A, Priotto G, Mattioli RC, Jannin JG. 2015.
779 Monitoring the Progress towards the Elimination of Gambiense Human African Trypanosomia-
780 sis. *PLoS Negl Trop Dis* 9:e0003785.
- 781 3. Mesu VKBK, Kalonji WM, Bardonneau C, Mordt OV, Blesson S, Simon F, Delhomme S,
782 Bernhard S, Kuziena W, Lubaki J-PF, Vuvu SL, Ngima PN, Mbembo HM, Ilunga M, Bonama
783 AK, Heradi JA, Solomo JLL, Mandula G, Badibabi LK, Dama FR, Lukula PK, Tete DN, Lum-
784 bala C, Scherrer B, Strub-Wourgaft N, Tarral A. 2018. Oral fexinidazole for late-stage African
785 *Trypanosoma brucei gambiense* trypanosomiasis: a pivotal multicentre, randomised, non-
786 inferiority trial. *Lancet* 391:144–154.
- 787 4. Deeks ED. 2019. Fexinidazole: First Global Approval. *Drugs* 79:215–220.
- 788 5. Keating J, Yukich JO, Sutherland CS, Woods G, Tediosi F. 2015. Human African trypanosomi-
789 asis prevention, treatment and control costs: a systematic review. *Acta Trop* 150:4–13.
- 790 6. Scott V, Sherwin T, Gull K. 1997. gamma-tubulin in trypanosomes: molecular characterisation
791 and localisation to multiple and diverse microtubule organising centres. *Journal of cell science*
792 110 (Pt 2):157–68.
- 793 7. Bastin P, Sherwin T, Gull K. 1998. Paraflagellar rod is vital for trypanosome motility. *Nature*
794 391:548.

- 795 8. Bastin P, Pullen TJ, Sherwin T, Gull K. 1999. Protein transport and flagellum assembly dynam-
796 ics revealed by analysis of the paralysed trypanosome mutant *snl-1*. *Journal of cell science* 112 (
797 Pt 21):3769–77.
- 798 9. Kohl L, Sherwin T, Gull K. 1999. Assembly of the paraflagellar rod and the flagellum attach-
799 ment zone complex during the *Trypanosoma brucei* cell cycle. *J Eukaryot Microbiol* 46:105–9.
- 800 10. Moreira-Leite FF, Sherwin T, Kohl L, Gull K. 2001. A trypanosome structure involved in
801 transmitting cytoplasmic information during cell division. *Science* (New York, NY 294:610–2.
- 802 11. Robinson DR, Gull K. 1991. Basal body movements as a mechanism for mitochondrial genome
803 segregation in the trypanosome cell cycle. *Nature* 352:731–3.
- 804 12. Vedrenne C, Giroud C, Robinson DR, Besteiro S, Bosc C, Bringaud F, Baltz T. 2002. Two re-
805 lated subpellicular cytoskeleton-associated proteins in *Trypanosoma brucei* stabilize microtu-
806 bles. *Molecular biology of the cell* 13:1058–70.
- 807 13. Pradel LC, Bonhivers M, Landrein N, Robinson DR. 2006. NIMA-related kinase TbNRKC is
808 involved in basal body separation in *Trypanosoma brucei*. *Journal of cell science* 119:1852–63.
- 809 14. Bonhivers M, Nowacki S, Landrein N, Robinson DR. 2008. Biogenesis of the trypanosome
810 endo-exocytotic organelle is cytoskeleton mediated. *PLoS Biol* 6:e105.
- 811 15. Henley GL, Lee CM, Takeuchi A. 1978. Electron microscopy observations on *Trypanosoma*
812 *brucei*: freeze-cleaving and thin-sectioning study of the apical part of the flagellar pocket. *Z*
813 *Parasitenkd* 55:181–7.
- 814 16. Webster P, Russell DG. 1993. The flagellar pocket of trypanosomatids. *Parasitology today* (Per-
815 sonal ed 9:201–6.

- 816 17. Morgan GW, Hall BS, Denny PW, Carrington M, Field MC. 2002. The kinetoplastida endo-
817 cytic apparatus. Part I: a dynamic system for nutrition and evasion of host defences. Trends in
818 parasitology 18:491–6.
- 819 18. Field MC, Carrington M. 2009. The trypanosome flagellar pocket. Nature reviews 7:775–86.
- 820 19. Alcantara C de L, Vidal JC, de Souza W, Cunha-E-Silva NL. 2017. The cytostome-cytopharynx
821 complex of *Trypanosoma cruzi* epimastigotes disassembles during cell division. J Cell Sci
822 130:164–176.
- 823 20. Esson HJ, Morriswood B, Yavuz S, Vidilaseris K, Dong G, Warren G. 2012. Morphology of the
824 trypanosome bilobe, a novel cytoskeletal structure. Eukaryotic cell 11:761–72.
- 825 21. Vidilaseris K, Morriswood B, Kontaxis G, Dong G. 2014. Structure of the TbBILBO1 protein
826 N-terminal domain from *Trypanosoma brucei* reveals an essential requirement for a conserved
827 surface patch. J Biol Chem 289:3724–3735.
- 828 22. Vidilaseris K, Shimanovskaya E, Esson HJ, Morriswood B, Dong G. 2014. Assembly mecha-
829 nism of *Trypanosoma brucei* BILBO1, a multidomain cytoskeletal protein. J Biol Chem
830 289:23870–23881.
- 831 23. Florimond C, Sahin A, Vidilaseris K, Dong G, Landrein N, Dacheux D, Albisetti A, Byard EH,
832 Bonhivers M, Robinson DR. 2015. BILBO1 is a scaffold protein of the flagellar pocket collar in
833 the pathogen *Trypanosoma brucei*. PLoS Pathog 11:e1004654.
- 834 24. Perdomo D, Bonhivers M, Robinson DR. 2016. The Trypanosome Flagellar Pocket Collar and
835 Its Ring Forming Protein-TbBILBO1. Cells 5.
- 836 25. Albisetti A, Florimond C, Landrein N, Vidilaseris K, Eggenpieler M, Lesigang J, Dong G,
837 Robinson DR, Bonhivers M. 2017. Interaction between the flagellar pocket collar and the hook

- 838 complex via a novel microtubule-binding protein in *Trypanosoma brucei*. *PLoS Pathog*
839 13:e1006710.
- 840 26. Vidilaseris K, Landrein N, Pivovarova Y, Lesigang J, Aeksiri N, Robinson DR, Bonhivers M,
841 Dong G. 2020. Crystal structure of the N-terminal domain of the trypanosome flagellar protein
842 BILBO1 reveals a ubiquitin fold with a long structured loop for protein binding. *J Biol Chem*
843 295:1489–1499.
- 844 27. Isch C, Majneri P, Landrein N, Pivovarova Y, Lesigang J, Lauruol F, Robinson DR, Dong G,
845 Bonhivers M. 2021. Structural and functional studies of the first tripartite protein complex at the
846 *Trypanosoma brucei* flagellar pocket collar. *PLoS Pathog* 17:e1009329.
- 847 28. Vickerman K. 1969. The fine structure of *Trypanosoma congolense* in its bloodstream phase. *J*
848 *Protozool* 16:54–69.
- 849 29. Dong X, Lim TK, Lin Q, He CY. 2020. Basal Body Protein TbSAF1 Is Required for Microtu-
850 bule Quartet Anchorage to the Basal Bodies in *Trypanosoma brucei*. *mBio* 11:e00668-20.
- 851 30. Gheiratmand L, Brasseur A, Zhou Q, He CY. 2013. Biochemical Characterization of the Bi-
852 lobe Reveals a Continuous Structural Network Linking the Bi-lobe to Other Single-copied Or-
853 ganelles in *Trypanosoma brucei*. *The Journal of biological chemistry* 288:3489–99.
- 854 31. Hamers-Casterman C, Atarhouch T, Muyldermans S, Robinson G, Hamers C, Songa EB, Ben-
855 dahman N, Hamers R. 1993. Naturally occurring antibodies devoid of light chains. *Nature*
856 363:446–448.
- 857 32. Greenberg AS, Avila D, Hughes M, Hughes A, McKinney EC, Flajnik MF. 1995. A new anti-
858 gen receptor gene family that undergoes rearrangement and extensive somatic diversification in
859 sharks. *Nature* 374:168–173.

- 860 33. Nguyen VK, Desmyter A, Muyldermans S. 2001. Functional heavy-chain antibodies in Cameli-
861 dae. *Adv Immunol* 79:261–296.
- 862 34. Holliger P, Hudson PJ. 2005. Engineered antibody fragments and the rise of single domains.
863 *Nat Biotechnol* 23:1126–1136.
- 864 35. Ward ES, Güssow D, Griffiths AD, Jones PT, Winter G. 1989. Binding activities of a repertoire
865 of single immunoglobulin variable domains secreted from *Escherichia coli*. *Nature* 341:544–
866 546.
- 867 36. Muyldermans S. 2013. Nanobodies: natural single-domain antibodies. *Annu Rev Biochem*
868 82:775–797.
- 869 37. Mir MA, Mehraj U, Sheikh BA, Hamdani SS. 2019. Nanobodies: The “magic bullets” in thera-
870apeutics, drug delivery and diagnostics. *Hum Antibodies* <https://doi.org/10.3233/HAB-190390>.
- 871 38. Matz H, Dooley H. 2019. Shark IgNAR-derived binding domains as potential diagnostic and
872 therapeutic agents. *Dev Comp Immunol* 90:100–107.
- 873 39. Woods J. 2019. Selection of Functional Intracellular Nanobodies. *SLAS Discov* 24:703–713.
- 874 40. Arias JL, Unciti-Broceta JD, Maceira J, Del Castillo T, Hernández-Quero J, Magez S, Soriano
875 M, García-Salcedo JA. 2015. Nanobody conjugated PLGA nanoparticles for active targeting of
876 African Trypanosomiasis. *J Control Release* 197:190–198.
- 877 41. Pardon E, Laeremans T, Triest S, Rasmussen SGF, Wohlkönig A, Ruf A, Muyldermans S, Hol
878 WGJ, Kobilka BK, Steyaert J. 2014. A general protocol for the generation of Nanobodies for
879 structural biology. *Nat Protoc* 9:674–693.

- 880 42. Van Audenhove I, Van Impe K, Ruano-Gallego D, De Clercq S, De Muynck K, Vanloo B, Ver-
881 straete H, Fernández LÁ, Gettemans J. 2013. Mapping cytoskeletal protein function in cells by
882 means of nanobodies. *Cytoskeleton (Hoboken)* 70:604–622.
- 883 43. Muyldermans S, Baral TN, Retamozzo VC, De Baetselier P, De Genst E, Kinne J, Leonhardt H,
884 Magez S, Nguyen VK, Revets H, Rothbauer U, Stijlemans B, Tillib S, Wernery U, Wyns L,
885 Hassanzadeh-Ghassabeh G, Saerens D. 2009. Camelid immunoglobulins and nanobody tech-
886 nology. *Vet Immunol Immunopathol* 128:178–83.
- 887 44. Abderrazek RB, Hmila I, Vincke C, Benlasfar Z, Pellis M, Dabbek H, Saerens D, El Ayeb M,
888 Muyldermans S, Bouhaouala-Zahar B. 2009. Identification of potent nanobodies to neutralize
889 the most poisonous polypeptide from scorpion venom. *The Biochemical journal* 424:263–72.
- 890 45. Kaplon H, Reichert JM. 2019. Antibodies to watch in 2019. *MAbs* 11:219–238.
- 891 46. Duggan S. 2018. Caplacizumab: First Global Approval. *Drugs* 78:1639–1642.
- 892 47. Morrison C. 2019. Nanobody approval gives domain antibodies a boost. *Nat Rev Drug Discov*
893 18:485–487.
- 894 48. Van Impe K, Bethuyne J, Cool S, Impens F, Ruano-Gallego D, De Wever O, Vanloo B, Van
895 Troys M, Lambein K, Boucherie C, Martens E, Zwaenepoel O, Hassanzadeh-Ghassabeh G,
896 Vandekerckhove J, Gevaert K, Fernández LÁ, Sanders NN, Gettemans J. 2013. A nanobody
897 targeting the F-actin capping protein CapG restrains breast cancer metastasis. *Breast Cancer*
898 *Res* 15:R116.
- 899 49. Meli G, Krako N, Manca A, Lecci A, Cattaneo A. 2013. Intrabodies for protein interference in
900 Alzheimer’s disease. *J Biol Regul Homeost Agents* 27:89–105.
- 901 50. Alirahimi E, Ashkiyan A, Kazemi-Lomedasht F, Azadmanesh K, Hosseininejad-Chafi M,
902 Habibi-Anbouhi M, Moazami R, Behdani M. 2017. Intrabody targeting vascular endothelial

903 growth factor receptor-2 mediates downregulation of surface localization. *Cancer Gene Ther*
904 24:33–37.

905 51. Aires da Silva F, Santa-Marta M, Freitas-Vieira A, Mascarenhas P, Barahona I, Moniz-Pereira
906 J, Gabuzda D, Goncalves J. 2004. Camelized rabbit-derived VH single-domain intrabodies
907 against Vif strongly neutralize HIV-1 infectivity. *Journal of molecular biology* 340:525–42.

908 52. Reimer E, Somplatzki S, Zegenhagen D, Hänel S, Fels A, Bollhorst T, Hovest LG, Bauer S,
909 Kirschning CJ, Böldicke T. 2013. Molecular cloning and characterization of a novel anti-TLR9
910 intrabody. *Cell Mol Biol Lett* 18:433–446.

911 53. Stijlemans B, Conrath K, Cortez-Retamozo V, Van Xong H, Wyns L, Senter P, Revets H, De
912 Baetselier P, Muyldermans S, Magez S. 2004. Efficient targeting of conserved cryptic epitopes
913 of infectious agents by single domain antibodies. African trypanosomes as paradigm. *J Biol*
914 *Chem* 279:1256–1261.

915 54. Baral TN, Magez S, Stijlemans B, Conrath K, Vanhollebeke B, Pays E, Muyldermans S, De
916 Baetselier P. 2006. Experimental therapy of African trypanosomiasis with a nanobody-
917 conjugated human trypanolytic factor. *Nat Med* 12:580–584.

918 55. Saerens D, Stijlemans B, Baral TN, Nguyen Thi GT, Wernery U, Magez S, De Baetselier P,
919 Muyldermans S, Conrath K. 2008. Parallel selection of multiple anti-infectome Nanobodies
920 without access to purified antigens. *J Immunol Methods* 329:138–50.

921 56. Stijlemans B, Caljon G, Natesan SKA, Saerens D, Conrath K, Pérez-Morga D, Skepper JN,
922 Nikolaou A, Brys L, Pays E, Magez S, Field MC, De Baetselier P, Muyldermans S. 2011. High
923 affinity nanobodies against the Trypanosome brucei VSG are potent trypanolytic agents that
924 block endocytosis. *PLoS Pathog* 7:e1002072.

- 925 57. Caljon G, Caveliers V, Lahoutte T, Stijlemans B, Ghassabeh GH, Van Den Abbeele J, Smolders
926 I, De Baetselier P, Michotte Y, Muyldermans S, Magez S, Clinckers R. 2012. Using microdial-
927 ysis to analyse the passage of monovalent nanobodies through the blood-brain barrier. *Br J*
928 *Pharmacol* 165:2341–2353.
- 929 58. Caljon G, Stijlemans B, Saerens D, Van Den Abbeele J, Muyldermans S, Magez S, De Baet-
930 selier P. 2012. Affinity is an important determinant of the anti-trypanosome activity of nano-
931 bodies. *PLoS Negl Trop Dis*, 2012/11/15 ed. 6:e1902–e1902.
- 932 59. Ditlev SB, Florea R, Nielsen MA, Theander TG, Magez S, Boeuf P, Salanti A. 2014. Utilizing
933 nanobody technology to target non-immunodominant domains of VAR2CSA. *PLoS One*
934 9:e84981–e84981.
- 935 60. Obishakin E, Stijlemans B, Santi-Rocca J, Vandenberghe I, Devreese B, Muldermans S, Bastin
936 P, Magez S. 2014. Generation of a nanobody targeting the paraflagellar rod protein of trypano-
937 somes. *PLoS ONE* 9:e115893.
- 938 61. Unciti-Broceta JD, Arias JL, Maceira J, Soriano M, Ortiz-González M, Hernández-Quero J,
939 Muñoz-Torres M, de Koning HP, Magez S, Garcia-Salcedo JA. 2015. Specific Cell Targeting
940 Therapy Bypasses Drug Resistance Mechanisms in African Trypanosomiasis. *PLoS Pathog*
941 11:e1004942.
- 942 62. Odongo S, Sterckx YGJ, Stijlemans B, Pillay D, Baltz T, Muyldermans S, Magez S. 2016. An
943 Anti-proteome Nanobody Library Approach Yields a Specific Immunoassay for *Trypanosoma*
944 *congolense* Diagnosis Targeting Glycosomal Aldolase. *PLoS Negl Trop Dis* 10:e0004420.
- 945 63. Stijlemans B, De Baetselier P, Caljon G, Van Den Abbeele J, Van Ginderachter JA, Magez S.
946 2017. Nanobodies As Tools to Understand, Diagnose, and Treat African Trypanosomiasis.
947 *Front Immunol* 8:724.

- 948 64. Pinto Torres JE, Goossens J, Ding J, Li Z, Lu S, Vertommen D, Naniima P, Chen R, Muylder-
949 mans S, Sterckx YG-J, Magez S. 2018. Development of a Nanobody-based lateral flow assay to
950 detect active *Trypanosoma congolense* infections. *Sci Rep* 8:9019.
- 951 65. Marschall ALJ, Dübel S. 2016. Antibodies inside of a cell can change its outside: Can intra-
952 bodies provide a new therapeutic paradigm? *Comput Struct Biotechnol J* 14:304–308.
- 953 66. Messer A, Joshi SN. 2013. Intrabodies as neuroprotective therapeutics. *Neurotherapeutics*
954 10:447–458.
- 955 67. Alzogaray V, Danquah W, Aguirre A, Urrutia M, Berguer P, Garcia Vescovi E, Haag F, Koch-
956 Nolte F, Goldbaum FA. 2010. Single-domain llama antibodies as specific intracellular inhibi-
957 tors of SpvB, the actin ADP-ribosylating toxin of *Salmonella typhimurium*. *FASEB J*
958 <https://doi.org/fj.10-162958> [pii] 10.1096/fj.10-162958.
- 959 68. Zhou C, Przedborski S. 2009. Intrabody and Parkinson's disease. *Biochimica et biophysica acta*
960 1792:634–42.
- 961 69. Koo MY, Park J, Lim JM, Joo SY, Shin S-P, Shim HB, Chung J, Kang D, Woo HA, Rhee SG.
962 2014. Selective inhibition of the function of tyrosine-phosphorylated STAT3 with a phosphory-
963 lation site-specific intrabody. *Proc Natl Acad Sci U S A*, 2014/04/14 ed. 111:6269–6274.
- 964 70. Stanimirovic D, Kemmerich K, Haqqani AS, Farrington GK. 2014. Engineering and pharma-
965 cology of blood-brain barrier-permeable bispecific antibodies. *Adv Pharmacol* 71:301–335.
- 966 71. Abulrob A, Sprong H, Van Bergen en Henegouwen P, Stanimirovic D. 2005. The blood-brain
967 barrier transmigrating single domain antibody: mechanisms of transport and antigenic epitopes
968 in human brain endothelial cells. *J Neurochem* 95:1201–1214.
- 969 72. Negi SS, Braun W. 2017. Cross-React: a new structural bioinformatics method for predicting
970 allergen cross-reactivity. *Bioinformatics* 33:1014–1020.

- 971 73. Faktorová D, Nisbet RER, Fernández Robledo JA, Casacuberta E, Sudek L, Allen AE, Ares M
972 Jr, Aresté C, Balestreri C, Barbrook AC, Beardslee P, Bender S, Booth DS, Bouget F-Y, Bow-
973 ler C, Breglia SA, Brownlee C, Burger G, Cerutti H, Cesaroni R, Chiurillo MA, Clemente T,
974 Coles DB, Collier JL, Cooney EC, Coyne K, Docampo R, Dupont CL, Edgcomb V, Einarsson
975 E, Elustondo PA, Federici F, Freire-Beneitez V, Freyria NJ, Fukuda K, García PA, Girguis PR,
976 Gomaa F, Gornik SG, Guo J, Hampl V, Hanawa Y, Haro-Contreras ER, Hehenberger E, High-
977 field A, Hirakawa Y, Hopes A, Howe CJ, Hu I, Ibañez J, Irwin NAT, Ishii Y, Janowicz NE,
978 Jones AC, Kachale A, Fujimura-Kamada K, Kaur B, Kaye JZ, Kazana E, Keeling PJ, King N,
979 Klobutcher LA, Lander N, Lassadi I, Li Z, Lin S, Lozano J-C, Luan F, Maruyama S, Matute T,
980 Miceli C, Minagawa J, Moosburner M, Najle SR, Nanjappa D, Nimmo IC, Noble L, Novák
981 Vanclová AMG, Nowacki M, Nuñez I, Pain A, Piersanti A, Pucciarelli S, Pyrih J, Rest JS, Rius
982 M, Robertson D, Ruaud A, Ruiz-Trillo I, Sigg MA, Silver PA, Slamovits CH, Jason Smith G,
983 Sprecher BN, Stern R, Swart EC, Tsaousis AD, Tsy-pin L, Turkewitz A, Turnšek J, Valach M,
984 Vergé V, von Dassow P, von der Haar T, Waller RF, Wang L, Wen X, Wheeler G, Woods A,
985 Zhang H, Mock T, Worden AZ, Lukeš J. 2020. Genetic tool development in marine protists:
986 emerging model organisms for experimental cell biology. *Nat Methods*, 2020/04/06 ed. 17:481–
987 494.
- 988 74. Bonhivers M, Nowacki S, Landrein N, Robinson DR. 2008. Biogenesis of the trypanosome
989 endo-exocytotic organelle is cytoskeleton mediated. *PLoS Biol* 6:e105.
- 990 75. Bianchini P, Peres C, Oneto M, Galiani S, Vicidomini G, Diaspro A. 2015. STED nanoscopy: a
991 glimpse into the future. *Cell Tissue Res* 360:143–150.
- 992 76. Wheeler RJ, Gull K, Sunter JD. 2019. Coordination of the Cell Cycle in Trypanosomes. *Annu*
993 *Rev Microbiol* 73:133–154.

- 994 77. Isch C, Majneri P, Landrein N, Pivovarova Y, Lesigang J, Lauruol F, Robinson DR, Dong G,
995 Bonhivers M. 2021. Structural and functional studies of the first tripartite protein complex at the
996 *Trypanosoma brucei* flagellar pocket collar. *PLoS Pathog* 17:e1009329.
- 997 78. Morriswood B, Havlicek K, Demmel L, Yavuz S, Sealey-Cardona M, Vidilaseris K, Anrather
998 D, Kostan J, Djinovic-Carugo K, Roux KJ, Warren G. 2013. Novel Bilobe Components in
999 *Trypanosoma brucei* Identified Using Proximity-Dependent Biotinylation. *Eukaryotic cell*
1000 12:356–67.
- 1001 79. Morriswood B, He CY, Sealey-Cardona M, Yelinek J, Pypaert M, Warren G. 2009. The bilobe
1002 structure of *Trypanosoma brucei* contains a MORN-repeat protein. *Molecular and biochemical*
1003 *parasitology* 167:95–103.
- 1004 80. Morriswood B, Schmidt K. 2015. A MORN Repeat Protein Facilitates Protein Entry into the
1005 Flagellar Pocket of *Trypanosoma brucei*. *Eukaryotic Cell* 14:1081–1093.
- 1006 81. Bastin P, MacRae TH, Francis SB, Matthews KR, Gull K. 1999. Flagellar morphogenesis: pro-
1007 tein targeting and assembly in the paraflagellar rod of trypanosomes. *Molecular and cellular bi-*
1008 *ology* 19:8191–200.
- 1009 82. Dang HQ, Zhou Q, Rowlett VW, Hu H, Lee KJ, Margolin W, Li Z. 2017. Proximity Interac-
1010 tions among Basal Body Components in *Trypanosoma brucei* Identify Novel Regulators of Ba-
1011 sal Body Biogenesis and Inheritance. *mBio* 8.
- 1012 83. Van den Abbeele A, De Clercq S, De Ganck A, De Corte V, Van Loo B, Soror SH, Srinivasan
1013 V, Steyaert J, Vandekerckhove J, Gettemans J. 2010. A llama-derived gelsolin single-domain
1014 antibody blocks gelsolin-G-actin interaction. *Cell Mol Life Sci* 67:1519–1535.

- 1015 84. De Vooght L, Caljon G, Stijlemans B, De Baetselier P, Coosemans M, Van den Abbeele J.
1016 2012. Expression and extracellular release of a functional anti-trypanosome Nanobody® in *Sodalis*
1017 *glossinidius*, a bacterial symbiont of the tsetse fly. *Microb Cell Fact* 11:23.
- 1018 85. De Vooght L, Caljon G, De Ridder K, Van Den Abbeele J. 2014. Delivery of a functional anti-
1019 trypanosome Nanobody in different tsetse fly tissues via a bacterial symbiont, *Sodalis*
1020 *glossinidius*. *Microb Cell Fact* 13:156–156.
- 1021 86. Böldicke T. 2017. Single domain antibodies for the knockdown of cytosolic and nuclear pro-
1022 teins. *Protein Sci*, 2017/03/24 ed. 26:925–945.
- 1023 87. Wirtz E, Leal S, Ochatt C, Cross GA. 1999. A tightly regulated inducible expression system for
1024 conditional gene knock-outs and dominant-negative genetics in *Trypanosoma brucei*. *Molecular*
1025 *and biochemical parasitology* 99:89–101.
- 1026 88. Nossal NG, Heppel LA. 1966. The release of enzymes by osmotic shock from *Escherichia coli*
1027 in exponential phase. *J Biol Chem* 241:3055–3062.
- 1028 89. Karlsson R, Katsamba PS, Nordin H, Pol E, Myszka DG. 2006. Analyzing a kinetic titration
1029 series using affinity biosensors. *Anal Biochem* 349:136–147.
- 1030 90. Palau W, Di Primo C. 2012. Single-cycle kinetic analysis of ternary DNA complexes by surface
1031 plasmon resonance on a decaying surface. *Biochimie* 94:1891–1899.
- 1032 91. Schumann Burkard G, Jutzi P, Roditi I. 2011. Genome-wide RNAi screens in bloodstream form
1033 trypanosomes identify drug transporters. *Mol Biochem Parasitol* 175:91–94.
- 1034 92. Heldin CH, Johnsson A, Wennergren S, Wernstedt C, Betsholtz C, Westermark B. 1986. A hu-
1035 man osteosarcoma cell line secretes a growth factor structurally related to a homodimer of
1036 PDGF A-chains. *Nature* 319:511–4.

- 1037 93. Dacheux D, Landrein N, Thonnus M, Gilbert G, Sahin A, Wodrich H, Robinson DR, Bonhivers
1038 M. 2012. A MAP6-Related Protein Is Present in Protozoa and Is Involved in Flagellum Motili-
1039 ty. *PloS one* 7:e31344.
- 1040 94. Hannaert V, Albert M-A, Rigden DJ, da Silva Giotto MT, Thiemann O, Garratt RC, Van Roy J,
1041 Opperdoes FR, Michels PAM. 2003. Kinetic characterization, structure modelling studies and
1042 crystallization of *Trypanosoma brucei* enolase. *Eur J Biochem* 270:3205–3213.
- 1043 95. Woods A, Sherwin T, Sasse R, MacRae TH, Baines AJ, Gull K. 1989. Definition of individual
1044 components within the cytoskeleton of *Trypanosoma brucei* by a library of monoclonal antibod-
1045 ies. *Journal of cell science* 93 (Pt 3):491–500.
- 1046
- 1047
- 1048
- 1049
- 1050
- 1051
- 1052
- 1053
- 1054
- 1055

1056 **Figure legends**

1057

1058 **Fig 1. Nanobodies as *TbBILBO1* immunofluorescence detection tools**

1059 (A) IFA testing of purified Nb48::HA::6His (green) on wild-type (WT) *T. brucei* cytoskeletons show-
1060 ing co-localization with *TbBILBO1* (probed with anti-*TbBILBO1* aa1-110 rabbit; red). The arrow
1061 indicates the FPC and the asterisk indicates co-labelling on the MTQ; both of these structures are
1062 co-labelled. (B) Purified Nb9::HA::6His does not label endogenous *TbBILBO1* in WT cytoskeletons.
1063 (C) Nb9::HA::6His on *T. brucei* over-expressing *TbBILBO1* (++) shows co-localization with
1064 *TbBILBO1*. (D) Purified Nb73::HA::6His on WT cytoskeletons does not label *TbBILBO1*. Scale bar
1065 = 5µm, inset = 1µm. For the sake of convenience, the proteins being probed in all figures are named
1066 as anti-Nb, plus the relevant nanobody name rather than its tag.

1067

1068 **Fig 2. Anti-*TbBILBO1* nanobodies Nb48::HA::6His and Nb9::HA::6His bind to *TbBILBO1* *in***
1069 ***vitro***

1070 (A) and (B) show WT, PCF cytoskeletons probed with Nb48::HA::6His followed by anti-HA, then
1071 FITC conjugated anti-mouse. (A) is a parasite cell in the 1K1N stage of the cell cycle. (B) is a cell
1072 in the 2K1N stage. Both cell stages show Nb48::HA::6His labelling on the FPC (black arrow) and MtQ
1073 (white asterisk). The MtQ signal was not always apparent on every cell imaged, which could be due
1074 to modulations between cell cycle stages. (C) WT, *T. brucei* cytoskeleton probed with anti-
1075 *TbBILBO1* (1-110) followed by anti-rabbit Alexa fluor 594. (D) WT cytoskeleton probed with anti-
1076 *TbBILBO1* and Nb48::HA::6His showing complete co-localization. (E) Western blot analysis of whole
1077 cell extracts of *T. brucei* PCF cells expressing *TbBILBO1* full-length (FL) and *TbBILBO1* trunca-
1078 tions, probed with Nb48::HA::6His. Non-induced (NI) and induced (I) trypanosomes expressing
1079 *TbBILBO1*::3cMyc FL protein, aa 171-587 (T3), and aa 251-587 (T4) were positive when probed with
1080 purified Nb48::HA::6His. (F) Western blot analysis of whole cell extracts of *T. brucei* PCF cells ex-

1081 pressing *TbBILBO1* full-length (FL) and *TbBILBO1* truncations probed with Nb9::*HA::6His*. Non-
1082 induced (NI) and induced (I) trypanosomes expressing *TbBILBO1::3cMyc* FL protein, aa 171-587
1083 (T3), and aa 251-587 (T4) were positive when probed with purified Nb9::*HA::6His*. Note: all proteins
1084 are running slightly faster than predicted size; FL should run at 70kDa, T3 should run at 49kDa and
1085 T4 at 40kDa. The black asterisk indicates labeling of endogenous *TbBILBO1* seen across all sam-
1086 ples. (G) A schematic diagram of cMyc tagged *TbBILBO1* full-length (FL) and truncations. Note
1087 that T1 and T2 are soluble. Nb9::*HA::6His* and Nb48::*HA::6His* bind to a region within aa 251 and 587 of
1088 *TbBILBO1*. (H) Kinetic analysis by surface plasmon resonance (SPR) of Nb9::*HA::6His* and (I)
1089 Nb48::*HA::6His*, binding to *6His::TbBILBO1*. The results of Nb9::*HA::6His* and Nb48::*HA::6His* binding are
1090 shown on the sensorgrams respectively, and are represented by the red curves. The black lines rep-
1091 resent the theoretical fit of each Nb as obtained from the Biaevaluation software to a kinetic titration
1092 data set of three concentrations of the nanobodies *in vitro*. Nb9::*HA::6His* displays a good affinity for
1093 *6His::TbBILBO1* with a K_D of 15.2 ± 0.7 nM, however, Nb48::*HA::6His* displays the highest affinity for
1094 *6His::TbBILBO1* with a K_D of 8.8 ± 0.7 nM. Scale bar = 5 μ m, inset = 1 μ m.

1095

1096 **Fig 3. INb48::*3cMyc* binds to *TbBILBO1* *in vivo***

1097 (A) IFA co-localization of INb48::*3cMyc* with *TbBILBO1* on isolated *T. brucei* PCF flagella. Scale
1098 bar = 5 μ m, inset = 1 μ m. (B) Immuno-electron micrographs of a purified flagellum from a trypano-
1099 some expressing INb48::*3cMyc* for 24hpi showing clear co-localization of INb48::*3cMyc* (5nm gold
1100 beads = white arrow) with *TbBILBO1* (15nm gold beads = black arrow). Both 5nm and 15nm sized
1101 gold beads are also clearly visible on the MtQ. BB = Basal Body, PBB = Pro-Basal body, FPC =
1102 Flagellar Pocket Collar, MtQ = Microtubule Quartet, A= axoneme. Scale bar = 500nm, inset = 250
1103 nm.

1104

1105 **Fig 4. INb48::*3cMyc* expression is trypanocidal**

1106 (A) Growth curves of trypanosome cells expressing INb48::3cMyc. Tetracycline dose dependent ef-
1107 fect on trypanosome growth and cytotoxicity for INb48::3cMyc expression in PCF *T. brucei*. (B)
1108 INb48::3cMyc (group 1) expressed in PCF induces rapid decline in population growth followed by
1109 cell death, (C) INb9::3cMyc (group 2) expressed in PCF induces cell growth arrest and cell death,
1110 and (D) INb73::3cMyc (group 3) expressed in PCF has no effect on population growth. (E) Western
1111 blot of INb48::3cMyc, INb9::3cMyc and INb73::3cMyc expression in PCF showing expression only in
1112 induced cells. Rapid degradation of protein due to cell death at 48hpi is observed for INb48::3cMyc
1113 and INb9::3cMyc. Time post induction is in hours.

1114

1115 **Fig 5. INb48::3cMyc expression *in vivo* induces phenotypes resembling *TbBILBO1* RNAi**

1116 **knockdown**

1117 (A) IFA of non-induced (NI) PCF *T. brucei* cells probed with anti-cMyc as a probe for INb48::3cMyc
1118 (green) and anti-*TbBILBO1* (red), indicating the absence of INb48::3cMyc labelling in non-induced
1119 cells. (B) An INb48::3cMyc induced (Ind) *T. brucei* cell at 24hpi showing co-localisation of
1120 INb48::3cMyc (green) with a disorganized signal for *TbBILBO1* (linear polymer formation instead of
1121 the typical annular shape) and a posteriorly localised, detached new flagellum (labelled as NF). As-
1122 terisk (*) denote the presence of co-localisation of INb48::3cMyc and anti-*TbBILBO1*, which is ob-
1123 served on the old flagellum (labelled as OF) and at the base of the new detached flagellum (labelled
1124 as NF). (C) Non-induced (NI) trypanosome showing correct location of *TbMORN1* labelling (red)
1125 at the base of the flagellum (labelled as F), with the classic hook and shank composition; there is no
1126 anti-cMyc signal in this NI cell. (D) At 24hpi (Ind), INb48::3cMyc labelling (green) is seen in the
1127 location of the FPC with linear labeling extending a short way along the axoneme; *TbMORN1* la-
1128 belling has changed from the classic hook shape and is seen as an extended linear form extending

1129 distally from the FPC region along the direction of the old flagellum (OF). (E) Non-induced (NI)
1130 trypanosome showing typical labelling of *TbPFR2* (red) along the flagellum. (F) 24hpi Ind
1131 INb48::3cMyc (green) showing a trypanosome cell with both the old (OF) and new flagella (NF) la-
1132 belled with *TbPFR2*. INb48::3cMyc labelling is observed only at the old FPC extending along ante-
1133 riorly in this cell. (G) A non-induced (NI) trypanosome cell probed with anti-*TbBLD10* (red), label-
1134 ling both the mature and pro-basal bodies (BB) at the base of the flagellum. (H) At 24hpi (+Tet) of
1135 INb48::3cMyc (green), a detached new flagellum (NF) is seen at the tip of at an extended posterior
1136 end; anti-*TbBLD10* labelling is seen associated with both the new and old flagella (red);
1137 INb48::3cMyc labelling is seen mainly in the region of the FPC of the old flagellum (green). Scale
1138 bar = 5µm.

1139

1140 **Fig 6. INb48::3cMyc expression disrupts FPC and HC formation**

1141 (A) Transmission electron micrograph (TEM) of a thin section of a WT PCF *T. brucei* cell showing
1142 the typical flagellar pocket (FP) (*), the base of the flagellar pocket (white arrows), flagellar ax-
1143 oneme (A), and exit site of the axoneme from the FP membrane; the transition zone is indicated by
1144 a black arrow within the FP. (B) Illustrates a detached flagellum from a thin section of PCF cells
1145 expressing INb48::3cMyc 24hpi (+Tet). The FP has not been formed and microtubules are present
1146 where the FP membrane should be located (black arrowheads). The transition zone of the axoneme
1147 is outside the cell body (black arrow). (C) TEM of a thin section of a cell expressing INb48::3cMyc
1148 for 24hpi (+Tet), showing accumulation of intracellular vesicles. M = Mitochondrion, V = vesicles,
1149 F = flagellum. Scale bar = 1µm. (D) Immuno-electron micrograph (iEM) of isolated flagella of PCF
1150 *T. brucei* after 24hpi (+Tet) of INb48::3cMyc expression. INb48::3cMyc is observed (5nm gold beads
1151 = black arrowheads) co-localizing with anti-*TbBILBO1* (15nm gold beads = black arrows) on the
1152 MtQ between the BB and the expected location of the FPC; note that the FPC is absent. (E) IEM of

1153 isolated flagella of PCF *T. brucei* after 24hpi (+Tet) of INb48::3cMyc expression showing
1154 INb48::3cMyc (5nm gold beads = black arrowheads) on the MtQ and an abnormal elongated label-
1155 ling of *TbMORN1* (15nm gold beads = black arrows). Note that in trypanosome cells expressing
1156 INb48::3cMyc, the new FPC is absent and the Hook Complex that is normally represented by
1157 *TbMORN1* has lost its hook-shape. BB = Basal Body, PBB = Pro-Basal body, MtQ = Microtubule
1158 Quartet, A= axoneme, PMtQ = Presumed Pro-basal body MtQ. Scale bar = 500nm, inset scale bar =
1159 100nm.

1160

1161 **Fig 7. Expression of INb48::3cMyc disrupts the cell cycle in *T. brucei***

1162 (A) INb48::3cMyc expression disrupts cytokinesis in *T. brucei*. Bar graph to show the percentage of
1163 trypanosomes counted at each stage of the cell cycle for non-induced (-Tet, blue bars), 12 hpi (+Tet
1164 12h, orange bars) and 24 hpi (+Tet 24h, red bars) for INb48::3cMyc expression. Note that at 24hpi
1165 approximately 35% of cells have detached flagella. INb48::3cMyc expression leads to a decrease in
1166 1K1N and an increase in 2K1N, 2K2N, abnormal 1K2N and XKXN phenotypes. N=300 trypano-
1167 somes per time point and each time point has been completed in triplicate. (B) Distribution of 2K2N
1168 cells after INb48::3cMyc expression in *T. brucei* showing strong similarities to *TbBILBO1* RNAi
1169 knockdown. The 2K2N cells were subdivided into 5 categories according to the visual appearance
1170 of the cell *i.e.*, possessing a detached flagellum, an extended posterior end, abnormal positioning of
1171 the kinetoplast and nucleus. **** $p < 0.0001$.

1172

1173 **Fig 8. Nb48 and INb48::3HA bind to *TbBILBO1* in a heterologous system and INb48::3HA inter-**
1174 **feres with *TbBILBO1* polymer formation**

1175 (A) Illustrates a non-transfected U-2 OS cell extracted with Triton X-100, probed with anti-
1176 *TbBILBO1* (1-110 rabbit) and purified Nb48::HA::6His and revealed independently by anti-HA

1177 (mouse) and their respective secondary fluorophores: anti-rabbit, Alexa fluor 594 and anti-mouse,
1178 FITC-conjugated. No labelling is observed. (B) Illustrates a U-2 OS cell that is expressing FL
1179 *TbBILBO1* and probed as above. *TbBILBO1* forms polymers and Nb48::_{HA::6His} labels these poly-
1180 mers. (C) Illustrates a U-2 OS cell expressing mutated EF-hand domain 2 (Mut2EF-*TbBILBO1*)
1181 and probed as above. The typical spiral polymers of this mutant are formed and are co-labelled with
1182 rabbit 1-110 and Nb48::_{HA::6His}. (D and E) Illustrate *TbBILBO1* truncations T1 (aa 1-170) and T2 (aa
1183 1-250) which are both cytoplasmic and thus eliminated during detergent extraction and thus not
1184 labelled (F and G) Illustrate the typical signals observed when *TbBILBO1* truncations T3 (171-587
1185 aa) and T4 (251-587 aa) are expressed in U-2 OS; the resulting polymers formed are both positive
1186 for *TbBILBO1* (in this case anti-*TbBILBO1* mouse monoclonal, IgM) and Nb48::_{HA::6His} (anti-HA
1187 rabbit, IgG). The IgM was used here because it binds to the C-terminus whereas anti-*TbBILBO1* (1-
1188 110) binds to the N-terminus of *TbBILBO1*. (H - P) In all experiments INb48, *TbBILBO1*,
1189 *TbBILBO1* mutations and truncations were expressed in U-2 OS cells for 24h then processed for
1190 IFA. IFA of non-extracted U-2 OS cell expressing INb48::_{3HA} only, and probed with anti-*TbBILBO1*
1191 and anti-HA to detect the intrabody. This cell shows that INb48::_{3HA} is cytoplasmic. (I) Illustration
1192 of a cell expressing INb48::_{3HA} only and probed with anti-*TbBILBO1* and anti-HA after detergent
1193 extraction, showing that INb48::_{3HA} has been removed after extraction. (J) Illustration of a non-
1194 extracted cell expressing INb48::_{3HA} and FL-*TbBILBO1* simultaneously, and probed as in (H and I).
1195 It illustrates that INb48::_{3HA} binds to the *TbBILBO1* polymers. However, these polymers are differ-
1196 ent to WT polymers shown in (B), suggesting that INb48::_{3HA} affects normal *TbBILBO1* polymer
1197 formation. (K) Illustrates a cell treated as in (J) but detergent extracted, demonstrating that
1198 INb48::_{3HA} is not removed upon detergent extraction. (L) The cell in this image is simultaneously
1199 expressing an EF-hand domain 2 mutated form of *TbBILBO1* (Mut2-EFh) and INb48::_{3HA}. The typ-
1200 ical helical spirals formed by the Mut2-EFhand protein are not formed when bound by INb48::_{3HA},
1201 suggesting again that INb48::_{3HA} binding affects polymer formation. *TbBILBO1* proteins and
1202 INb48::_{3HA} were expressed in U-2 OS cells for 24h; in this case INb48::_{3HA}, was co-expressed T1-T4

1203 truncations. Cells were then processed for IFA using either the anti-*TbBILBO1* (1-110) rabbit poly-
1204 clonal, raised to and binding only, the N-terminus of *TbBILBO1*, for detecting T1 and T2, or an in-
1205 house made anti-*TbBILBO1* IgM mouse monoclonal, which recognizes the C' terminus of
1206 *TbBILBO1*; anti-HA was used to detect INb48::3HA followed by their respective secondary antibod-
1207 ies. (M) Illustrates an IFA image of a U-2 OS cell simultaneously expressing INb48::3HA and
1208 *TbBILBO1* T1. These images illustrate that INb48::3HA and T1 are both cytoplasmic and therefore
1209 give an overlapping signal. (N) Illustrates an IFA image of a U-2 OS cell simultaneously expressing
1210 INb48::3HA and *TbBILBO1* T2. Similar to (M) both of these proteins are cytoplasmic and give an
1211 overlapping signal. (O) This is a IFA image of a U-2 OS cell simultaneously expressing INb48::3HA
1212 and *TbBILBO1* T3. The typical linear filaments formed by T3 are modified when bound by
1213 INb48::3HA, suggesting the intrabody binding inhibits the typical polymer formation. (P) Illustrates
1214 detergent extracted IFA images of U-2 OS cells simultaneously expressing INb48::3HA and
1215 *TbBILBO1* T4. The spindle shaped polymers, as observed in Figure 8G, are observed to a lesser
1216 extent but numerous smaller polymers are present in the cytoplasm. These are never present in cells
1217 expressing T4 alone, suggesting that the binding of INb48 to T4 modifies the polymer forming ca-
1218 pacity of this truncation. Scale bar = 5µm.

1219

1220 **Supporting Information**

1221 **Sup Fig 1. Production and purification of Nb48, 9 and 73**

1222 (A) Coomassie blue stained gel of Nb48 expression before (NI) and after IPTG induction (I) and
1223 purification samples. Nb48 was obtained from elutions E2-E5. (FT = flow through, W = wash and
1224 E1-E5 = elution 1 to elution 5) in bacteria. (B) Coomassie blue stained gel of Nb9 expression in
1225 bacteria before (NI) and after IPTG induction (I) and purification. Nb9 was obtained from elutions
1226 E1-E5 and peaking at E3. (PE = periplasmic extract, FT = flow through and E1-E5 = elution 1 to
1227 elution 5). (C) Coomassie blue stained gel of Nb73 expression in bacteria before (NI) and after

1228 IPTG induction (I) and purification. Nb73 was obtained from elutions E2-E3. (FT = flow through,
1229 W = wash and E1-E5 = elution 1 to elution 5).

1230

1231 **Sup Fig. 2. Anti-*Tb*BILBO1 nanobodies: Western blotting, purification and use in IFA**

1232 (A) Bacterial expressed nanobody (Nb::*HA*::6His) samples probed on a WB with anti-*HA*. Samples of
1233 non-induced (NI), induced (I) bacterial cultures, pellet (P) and periplasmic extract (Ex). (B) Purifi-
1234 cation of Nb48::*HA*::6His : flow through (FT), wash (W) and elutions (lanes 1-6), all lanes were probed
1235 by WB using anti-His. (C) IFA controls for (Figure 2A-D and Figure 1). First panel is a WT *T.*
1236 *brucei*, procyclic, cytoskeleton probed with anti-rabbit Alexa fluor 594 followed by anti-mouse
1237 FITC but no primary antibodies, demonstrating that there is no cross-reaction between these sec-
1238 ondary antibodies or on the cytoskeleton. The second panel is a negative control of WT cytoskele-
1239 ton probed with anti-mouse FITC but no primary antibody, which demonstrates that there is no
1240 cross-reaction between this secondary antibody and the cytoskeleton. The third panel is a negative
1241 control of a WT cytoskeleton probed with anti-*HA* rabbit followed by anti-mouse FITC, which
1242 demonstrates that there is no cross-reaction between these antibodies on the cytoskeleton. (D) In
1243 non-induced INb48::*3cMyc* cells (first panel), anti-*cMyc* reveals no labeling. After INb48::*3cMyc* ex-
1244 pression is induced for 3 hours (+3h; second panel) labelling is visible at the FPC (green) co-
1245 localizing with *Tb*BILBO1 (red) at the FPC and along the MtQ (*). The two other panels show lo-
1246 calization of INb48::*3cMyc* (green) with *Tb*MORN1 (red) and *Tb*BLD10 (a basal body marker; red)
1247 respectively. (E) After 6 hours of INb9::*3cMyc* induction INb9 labelling is visible at the FPC
1248 (green) and co-localizes with *Tb*BILBO1 (red) at the FPC. Scale bar = 5µm, inset = 1µm.

1249

1250 **Sup Fig 3. Expression of control anti-GFP nanobody and 48h expression of INb48**

1251 (A) Growth curve of *T. brucei* PCF cells expressing INbGFP::*3cMyc*, show that expression of anti-
1252 GFP intrabody does not induce a cell growth phenotype. (B) Western blot of expression of IN-
1253 bGFP::*3cMyc* in *T. brucei* showing expression at 24 and 48hpi. *Tb*Enolase, is a cytoplasmic protein,

1254 that has been used as a loading control. (C) IFA of non-induced PCF *T. brucei* cells probed with
1255 anti-*TbBILBO1* (red) and anti-cMyc to label INbGFP::3cMyc (green - weak background signal) (non-
1256 induced NI; top panel). A trypanosome induced for 24h (+Tet) demonstrating cytoplasmic localisa-
1257 tion of INbGFP::3cMyc (green) and the normal FPC localisation of *TbBILBO1* (red) (Bottom panel).
1258 Scale bar = 5µm, in the insets the scale bar = 1µm. (D) IFA of a *T. brucei* PCF cell expressing
1259 INb48::3cMyc for 48h and probed with anti-cMyc (green) and anti-BILBO1 (red). Multiple detached
1260 flagella are observed in a single cell, with *TbBILBO1* labelling at two disrupted FPs. (E) As in D,
1261 but showing two very distorted FPC that consist of long polymers rather than the distinctive annular
1262 structure. For the sake of convenience, the protein being probed is named as anti-Nb, plus the rele-
1263 vant nanobody name rather than its tag. Scale bar = 5µm, inset = 1µm.

1264

1265 **Sup Fig 4. IFA antibody controls for expression of INb48::3HA and/or *TbBILBO1* in U-2 OS**

1266 **cells** Controls for Figure 8. (A) Images of a U-2 OS wild-type (WT) whole cell that has not been
1267 transfected with INb48::3HA or *TbBILBO1* and is probed with secondary antibodies only. No signal
1268 is observed. (B) Images of a U-2 OS whole cell that has been transfected with INb48::3HA and
1269 *TbBILBO1* and probed as in (A); no signal is observed. (C) Images of a U-2 OS whole cell that has
1270 been transfected with *TbBILBO1* full-length and probed as in (A); no signal is observed. (D) Imag-
1271 es of a U-2 OS whole cell that has been transfected with INb48::3HA and probed as in (A); no signal
1272 is observed. Scale bars = 5µm.

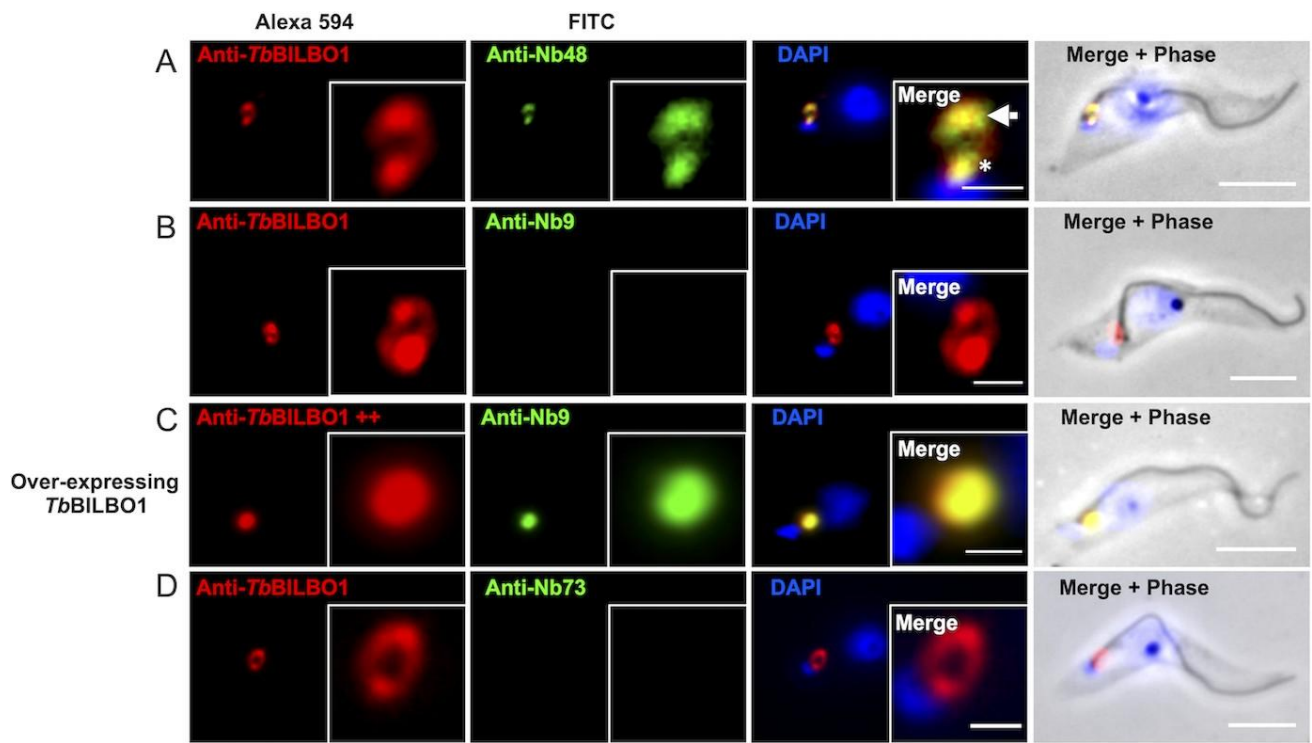
1273

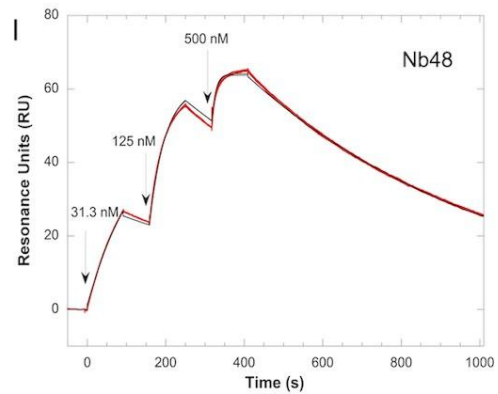
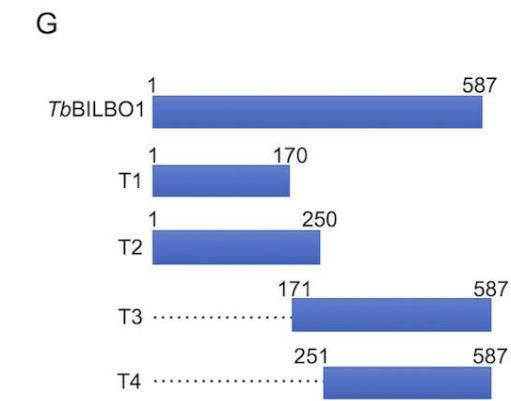
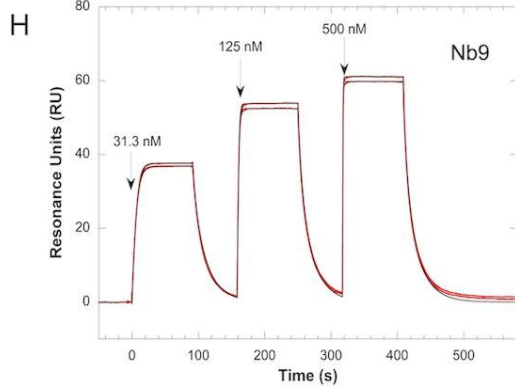
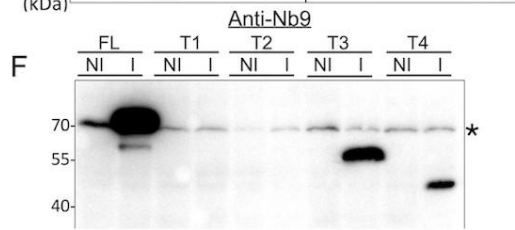
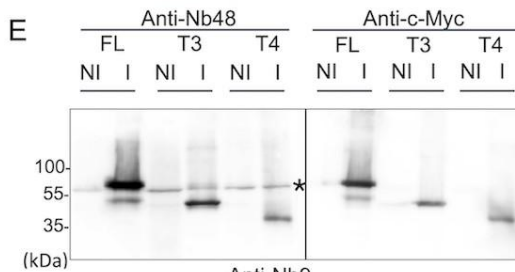
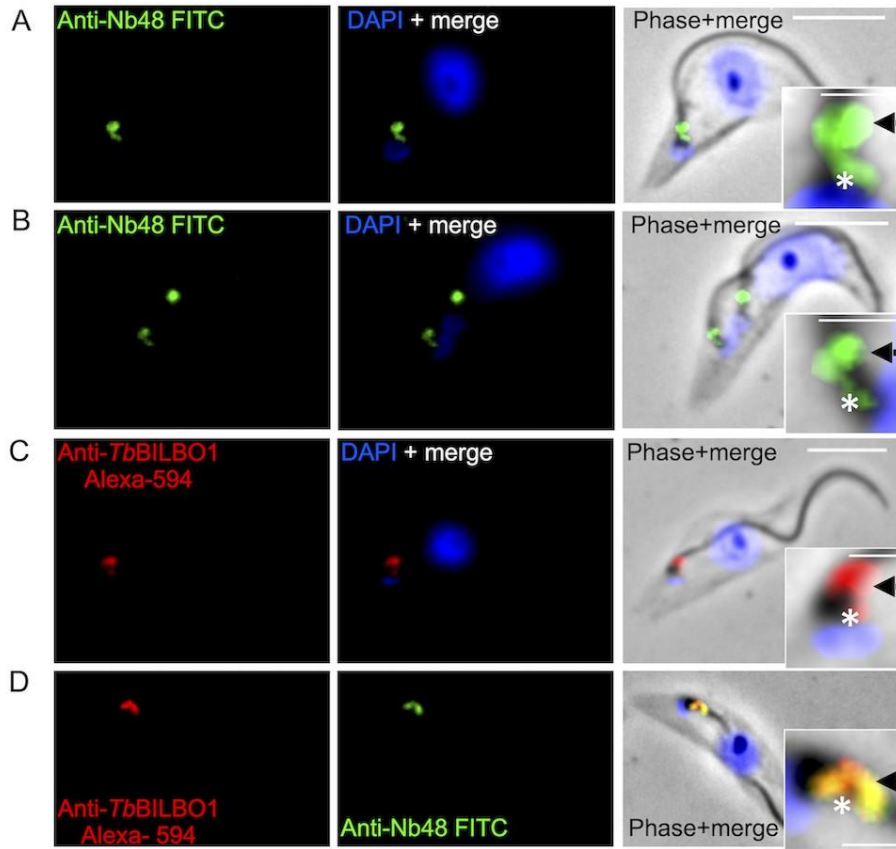
1274 **Sup Fig 5. Controls of intra-nanobody anti-GFP (INbGFP::3HA) and/or *TbBILBO1* expressed**
1275 **in U-2 OS cells**

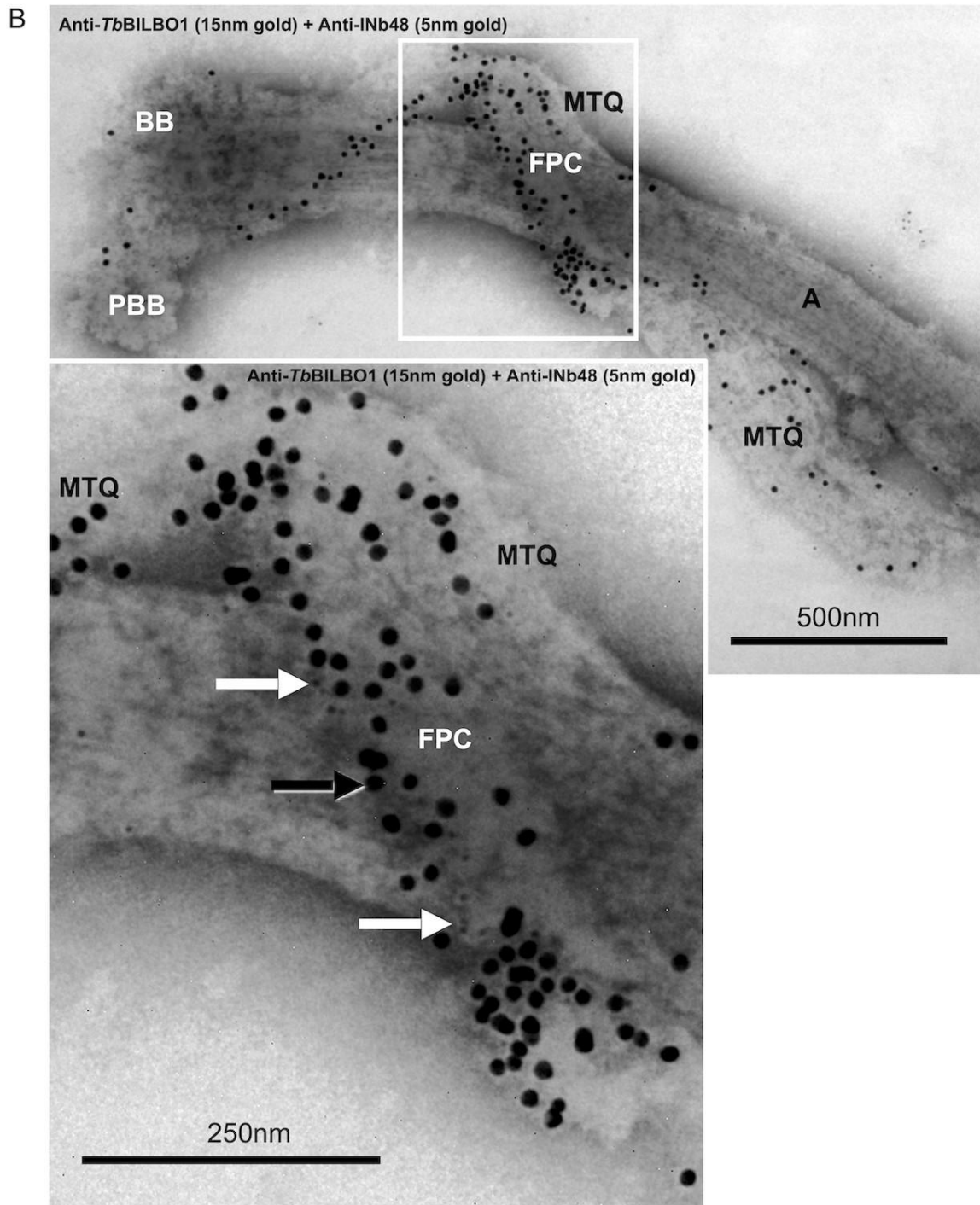
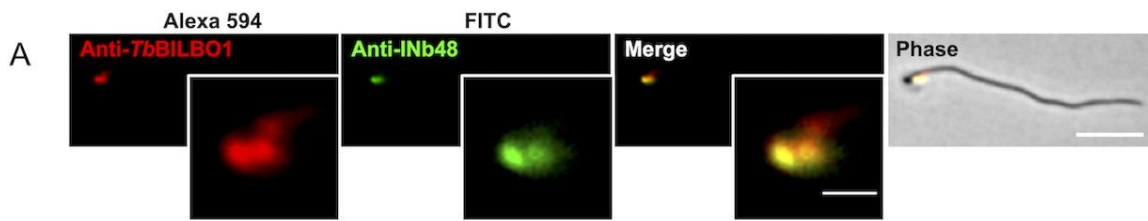
1276 (A) Images of antibody controls of intrabody anti-GFP (INbGFP::3HA) and *TbBILBO1* expressed in
1277 U-2 OS cells and probed with anti-HA, plus anti-*TbBILBO1* (1-110) followed by their respective
1278 secondary antibodies anti-rabbit Alexa 594 and anti-mouse FITC. Both *TbBILBO1* polymers and

1279 the cytoplasmic nanobody (INbGFP::*3HA*; green) are observed, but the GFP intrabody does not bind
1280 to *TbBILBO1* positive polymers (red). (B) Images of a cell treated and probed as in (A) but deter-
1281 gent extracted, illustrating that the anti-GFP intrabody is cytoplasmic and soluble and is removed by
1282 detergent extraction, but not the *TbBILBO1* polymers (red). (C) Images of a U-2 OS cell only ex-
1283 pressing the INbGFP::*3HA* but probed as in (A) and illustrating a green cytoplasmic labelling of the
1284 intrabody only, which does not form polymers. (D and E) Images of antibody controls of IN-
1285 bGFP::*3HA* and *TbBILBO1* expressed in U-2 OS cells and probed with secondary antibodies only:
1286 Alexa 594 and anti-mouse FITC. (D) is a whole cell whilst (E) is detergent extracted. No signal is
1287 observed in either cell. Scale bar = 5 μ m.

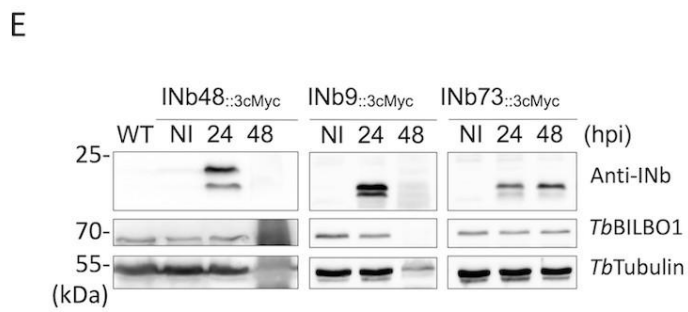
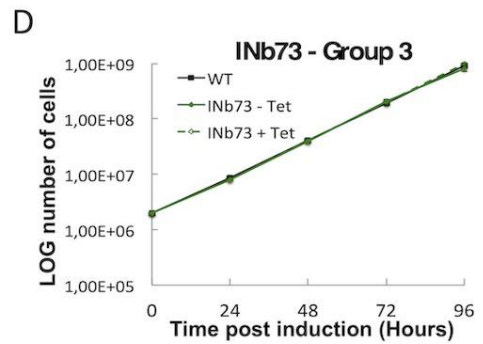
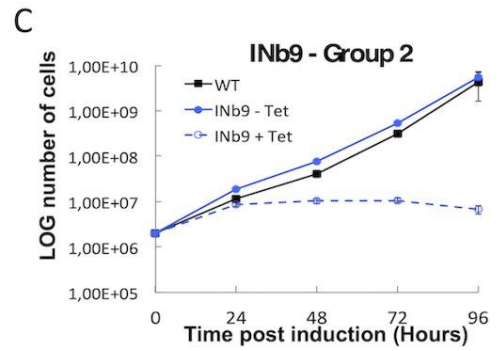
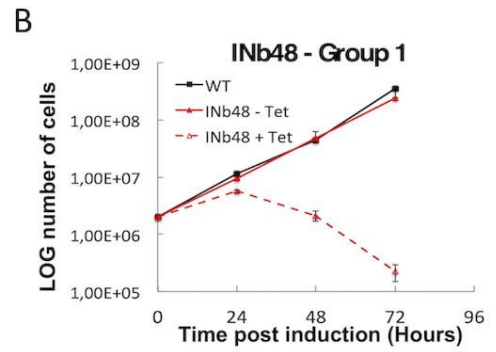
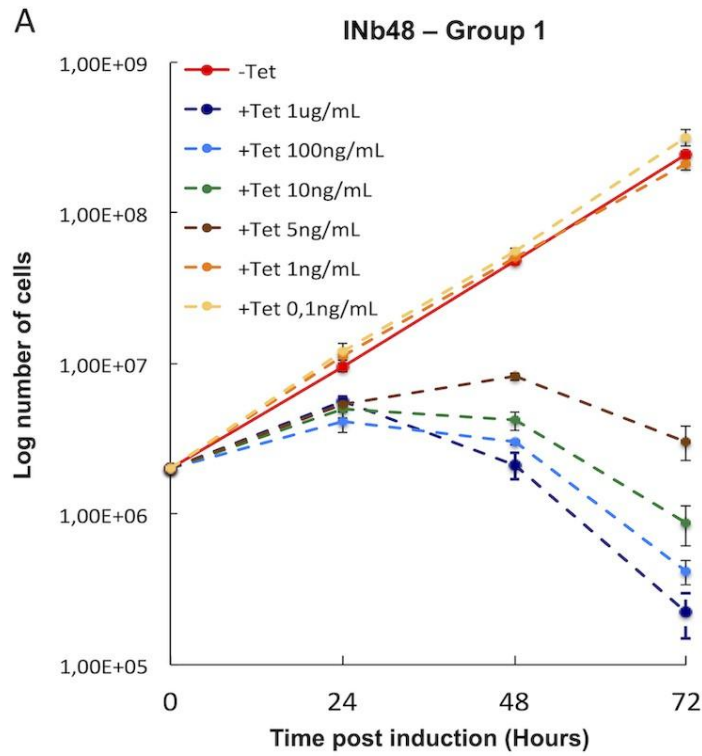
1288

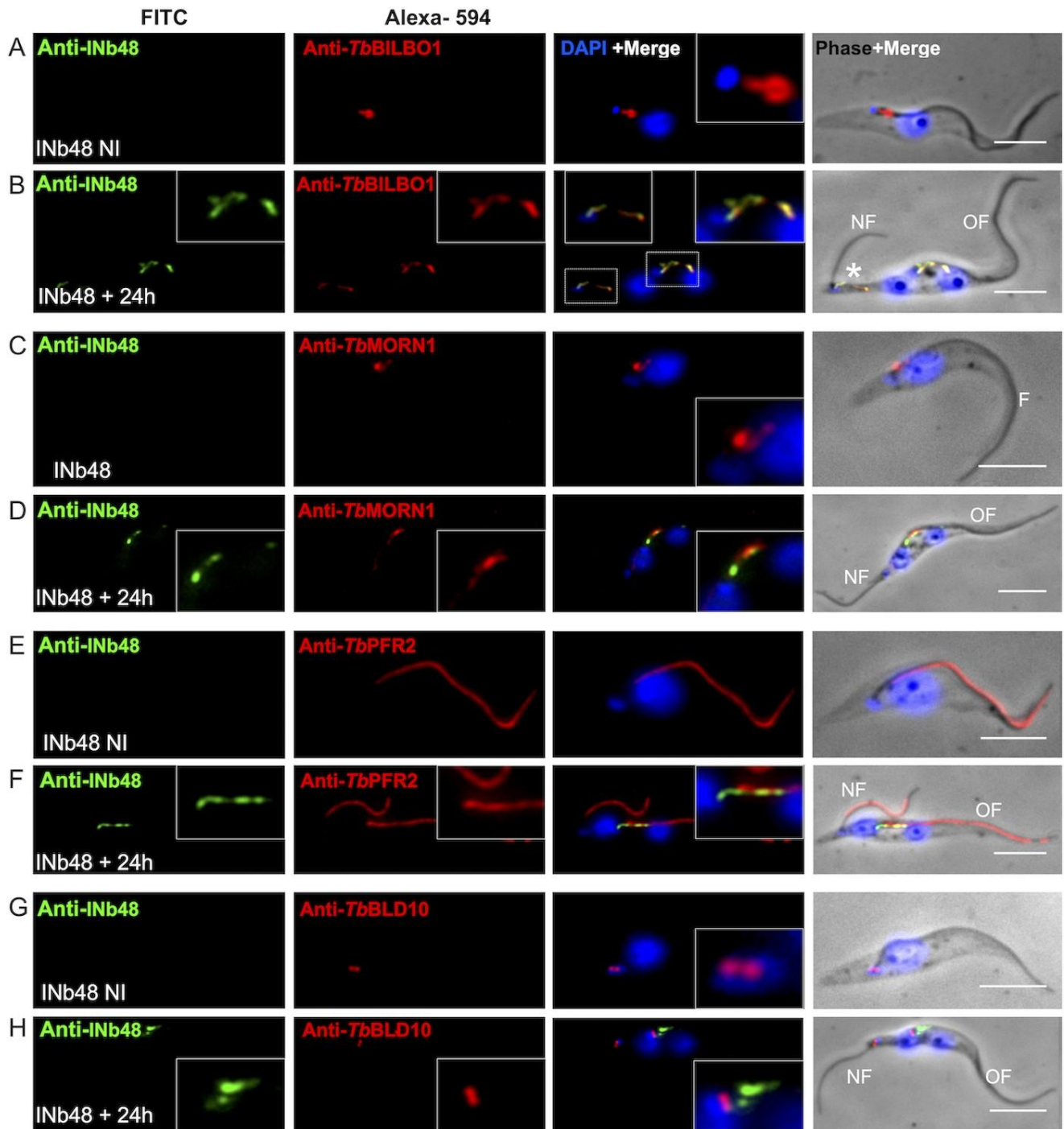


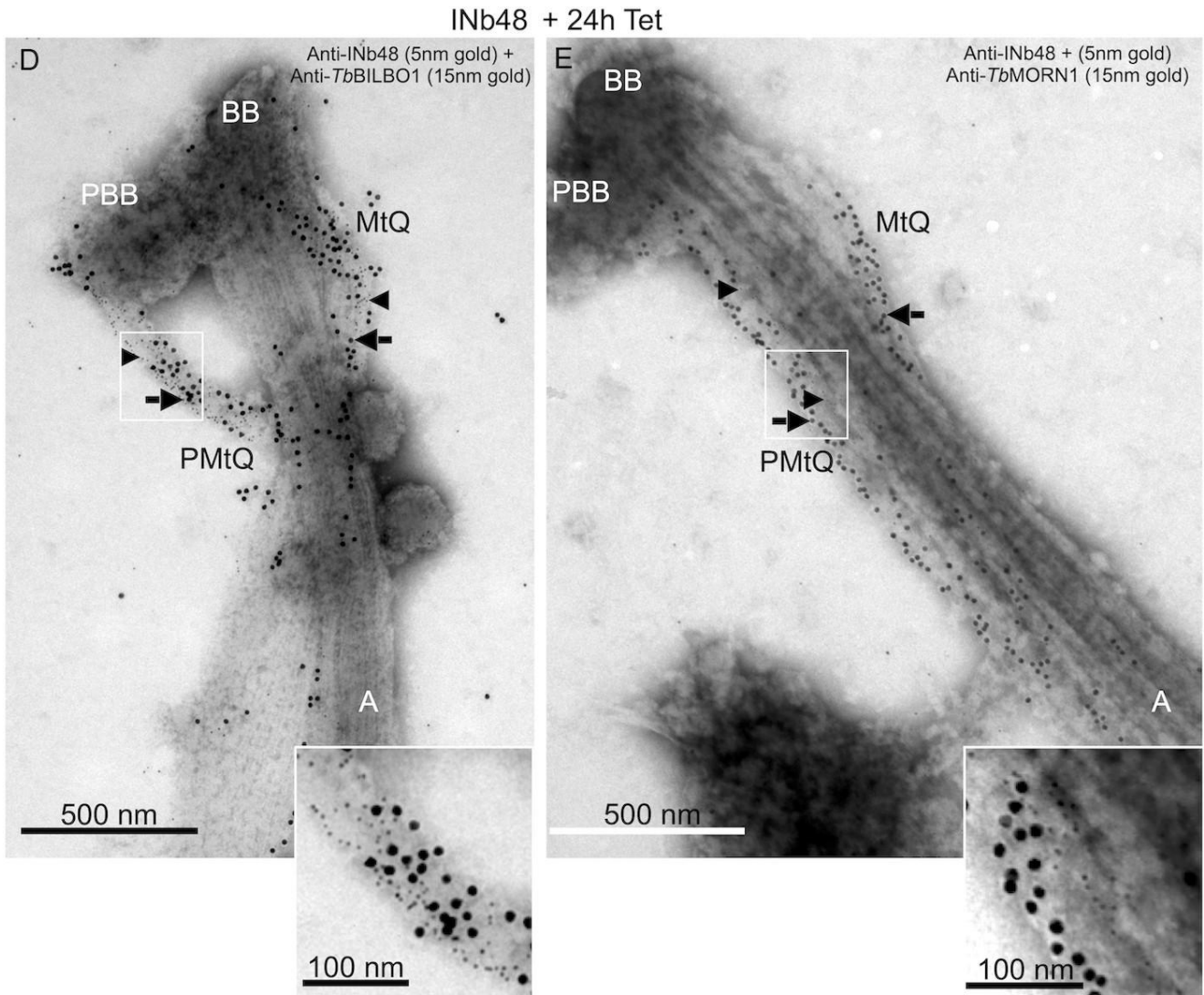
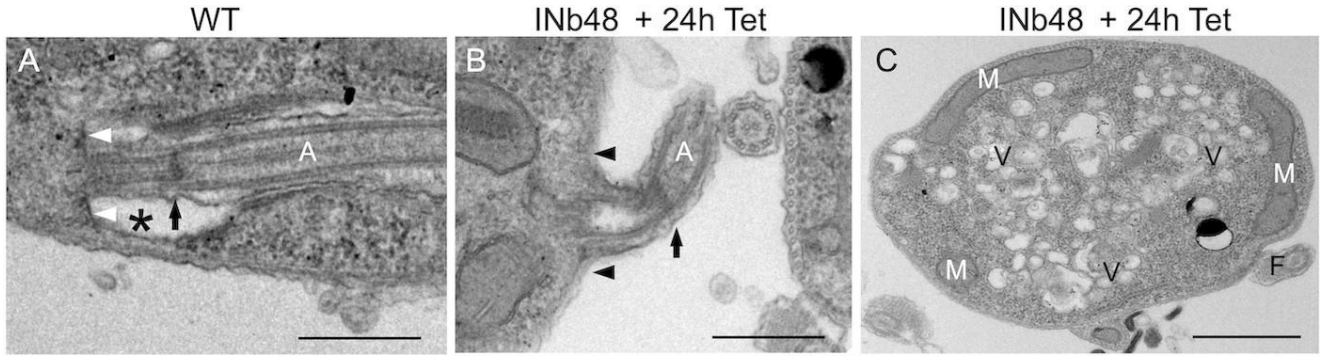




Anti-INb48 (5nm gold beads = white arrow)
Anti-TbBILBO1 (15nm gold beads = black arrow)

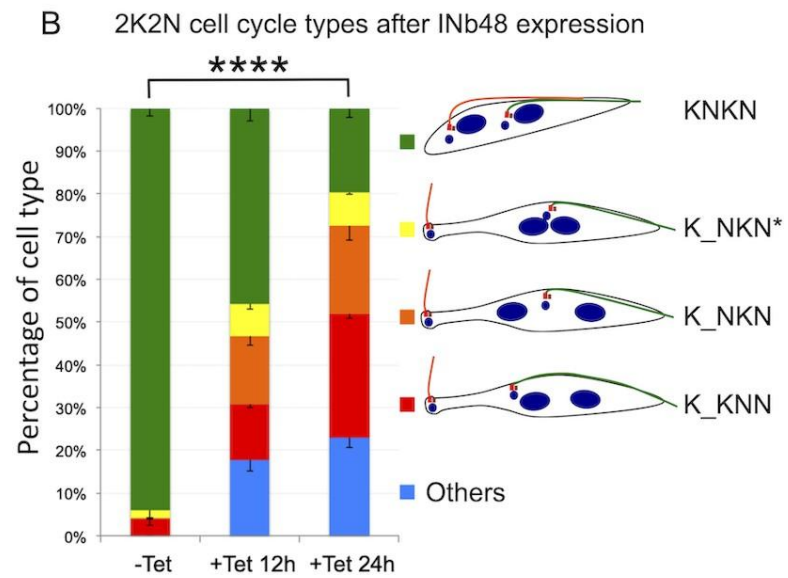
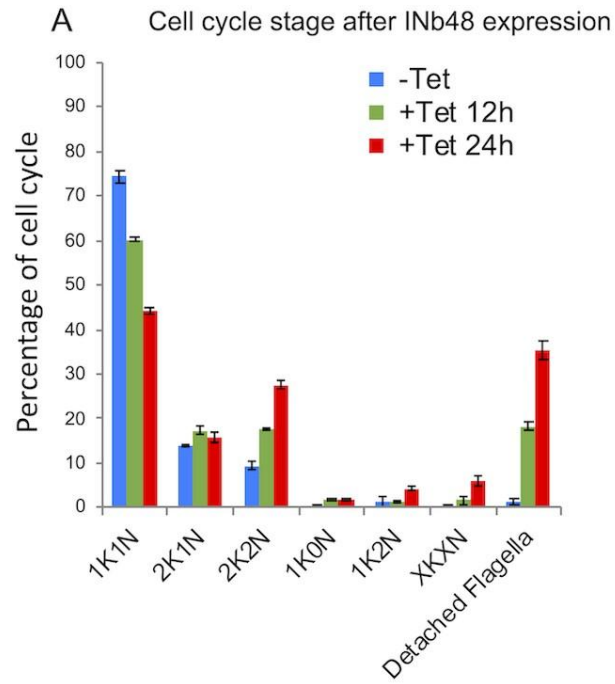


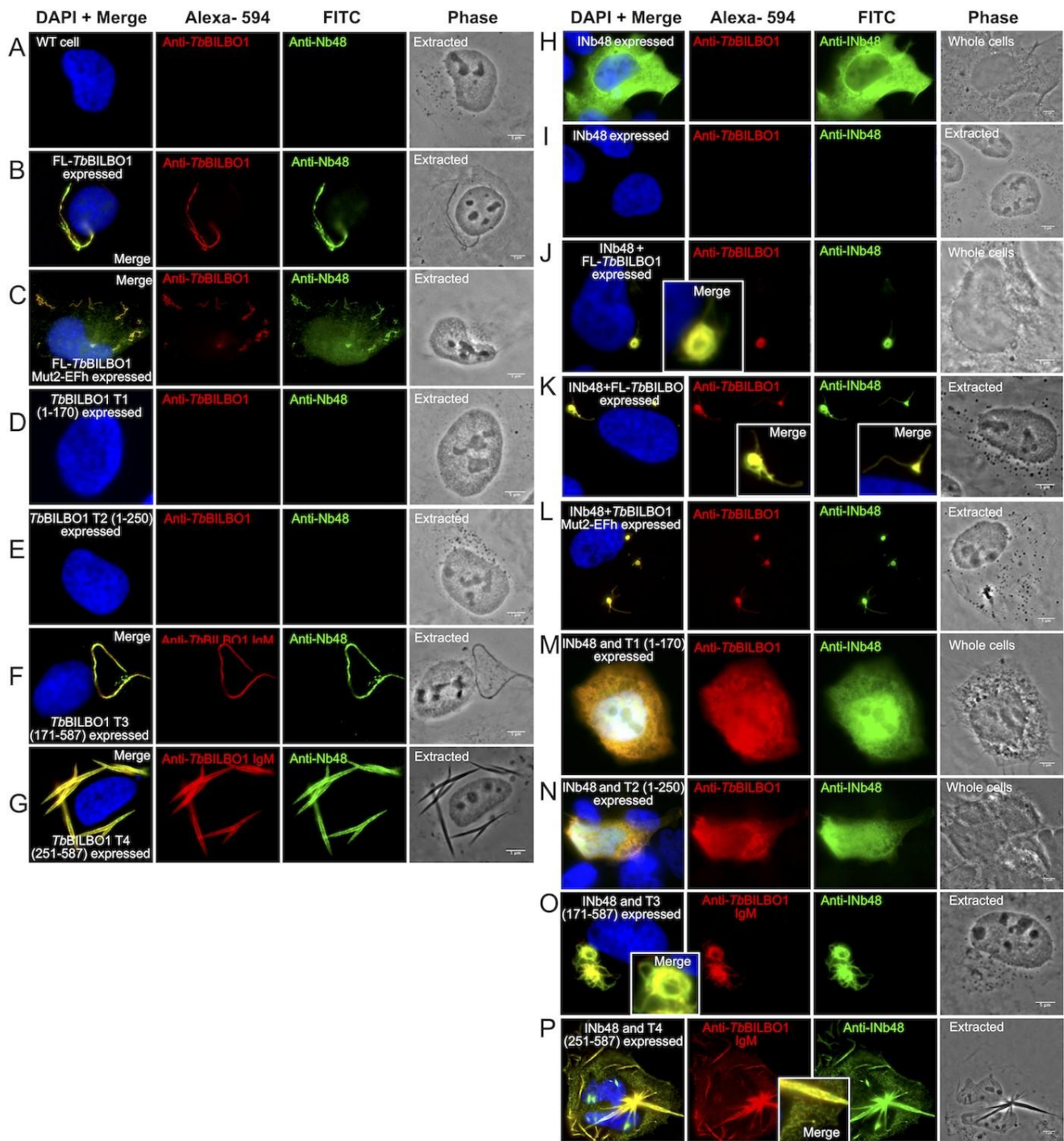




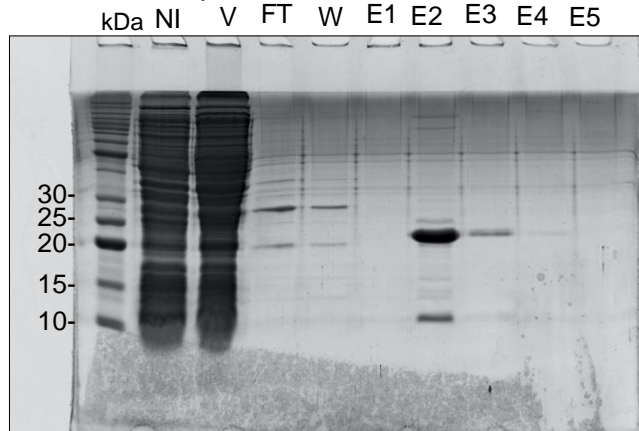
Anti-INb48 (5nm gold beads = black arrowheads)
Anti-TbBILBO1 1-110 (15nm gold beads = black arrows)

Anti-INb48 (5nm gold beads = black arrowheads)
Anti-TbMORN1 (15nm gold beads = black arrows)

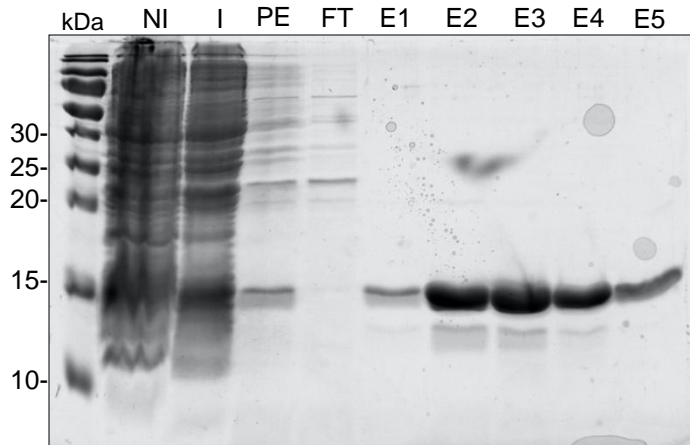




A Production and purification of **Nb48**: Coomassie gel



B Production and purification of **Nb9**: Coomassie gel



C Production and purification of **Nb73**: Coomassie gel

